Oil & Gas Science and Technology – Rev. IFP, Vol. 55 (2000), No. 4, pp. 359-393

A Scale-up Strategy for a Commercial Scale Bubble Column Slurry Reactor for Fischer-Tropsch Synthesis

R. Krishna[1]

1 Department of Chemical Engineering, University of Amsterdam, Nieuwe Achtergracht 166, 1018 WV Amsterdam - The Netherlands
e-mail: krishna@chemeng.chem.uva.nl

Résumé — Stratégie d'extrapolation vers un réacteur industriel de synthèse Fischer-Tropsch en colonne à bulles avec catalyseur en suspension — Les réacteurs à colonne à bulles trouvent de plus en plus d'applications dans l'industrie. Cette technologie est très en vue dans les procédés de transformation du gaz naturel en carburants liquides et en oléfines légères par le procédé de Fischer-Tropsch. On rencontre des problèmes considérables pour l'étude et l'extrapolation de ce type de réacteur. D'abord, il faut une grande capacité de traitement du gaz, ce qui nécessite l'emploi de réacteurs d'un grand diamètre, généralement de 5-8 m, souvent en parallèle. En deuxième lieu, le procédé fonctionne à haute pression, généralement 40 bar. Ensuite, pour obtenir un haut rendement, il est nécessaire d'avoir une grande hauteur de réacteur, généralement de 30-40 m, et d'utiliser des suspensions très concentrées, à presque 40 % en volume. Enfin, la nature exothermique du procédé exige d'insérer des tubes de refroidissement dans le réacteur pour évacuer la chaleur dégagée. La commercialisation de cette technologie dépend absolument d'une réelle compréhension des principes d'extrapolation des colonnes à bulles dans les conditions mentionnées ci-dessus, principes qui vont au-delà de la plupart des théories et des corrélations publiées.

Pour développer de véritables règles d'extrapolation de ces réacteurs avec catalyseur en suspension, nous avons réalisé un programme complet d'étude hydrodynamique (taux de rétention du gaz, distribution radiale des vitesses de liquide, mélange en retour des liquides) dans des colonnes ayant un diamètre de 0,05 ; 0,1 ; 0,15 ; 0,174 ; 0,19 ; 0,38 et 0,63 m. Pour la phase liquide, on a utilisé divers liquides (eau, tétradécane, paraffine, huile de Tellus). On a ajouté dans les paraffines des particules de silice à des concentrations allant jusqu'à environ 40 % en volume afin d'étudier l'hydrodynamique de la suspension. Une colonne de 0,15 m de diamètre a été mise sous des pressions de 0,1 à 1,3 MPa avec un système air/eau, et l'on a mesuré le taux de rétention du gaz et le transfert de masse gaz/liquide. De plus, une étude d'images vidéo a été réalisée sur une colonne rectangulaire à deux dimensions, pour étudier les caractéristiques de montée des bulles simples, les interactions entre les bulles, et les phénomènes de rupture et de coalescence.

Nos expériences montrent que le diamètre de la colonne, les pressions élevées et la concentration de la suspension exercent une influence importante sur l'hydrodynamique. Ces effets ne sont pas convenablement décrits dans les corrélations déjà publiées dans la littérature.

L'extrapolation des données obtenues dans des unités de laboratoire à froid vers des réacteurs à une échelle industrielle demande une approche systématique basée sur la compréhension des principes d'extrapolation de la dynamique des bulles et du comportement des dispersions à deux phases dans les colonnes à grande échelle.

Nous développons ici, pour l'extrapolation du réacteur à colonne à bulles, une approche à plusieurs niveaux reposant sur une combinaison d'expériences et soutenue par des simulations numériques de

dynamique des fluides (CFD, *Computational Fluid Dynamics*) pour la compréhension physique. Cette approche comprend les phases suivantes :

– description de la morphologie des bulles simples et de la dynamique de la montée — ici, on utilise à la fois les expériences et les simulations du volume de fluide (VOF, Volume of Fluid) ;
– modélisation des interactions entre les bulles ;
– description du comportement des nuages de bulles et du développement des relations d'échange de moment interfacial réel entre les bulles et le liquide ;
– simulations CFD dans un repère eulérien pour l'extrapolation des informations obtenues à l'échelle du laboratoire vers les réacteurs commerciaux à l'échelle industrielle.

Mots-clés : synthèse Fischer-Tropsch, colonne à bulles triphasique, régimes d'écoulement, stratégie d'extrapolation, taux de rétention, mélange, transfert de masse, modélisation.

Abstract — A Scale-up Strategy for a Commercial Scale Bubble Column Slurry Reactor for Fischer-Tropsch Synthesis *— Bubble column reactors are finding increasing use in industrial practice; this reactor technology figures prominently in processes for converting natural gas to liquid fuels and light olefins using Fischer-Tropsch synthesis. There are considerable reactor design and scale-up problems associated with the Fischer-Tropsch bubble column slurry reactor. Firstly, large gas throughputs are involved, necessitating the use of large diameter reactors, typically 5-8 m, often in parallel. Secondly, the process operates under high-pressure conditions, typically 40 bar. Thirdly, in order to obtain high conversion levels, large reactor heights, typically 30-40 m tall, are required along with the use of highly concentrated slurries, approaching 40 vol%. Finally, the process is exothermic in nature, requiring heat removal by means of cooling tubes inserted in the reactor. Successful commercialisation of this technology is crucially dependent on the proper understanding of the scaling-up principles of bubble columns for the above mentioned conditions which fall outside the purview of most published theory and correlations.*

In order to develop the proper scale-up rules for the bubble column slurry reactor we have undertaken a comprehensive program of investigation of the hydrodynamics (gas holdup, radial distribution of liquid velocities, backmixing of the liquid) in columns of diameters 0.05, 0.1, 0.15, 0.174, 0.19, 0.38 and 0.63 m. A variety of liquids (water, tetradecane, paraffin oil, Tellus oil) were used as the liquid phase. Silica particles in concentrations up to about 40 vol% were added to paraffin oil in order to study slurry hydrodynamics. One column of 0.15 m diameter was operated at pressures ranging from 0.1 to 1.3 MPa with the air-water system and the gas holdup and gas-liquid mass transfer were measured. Additionally, video imaging studies in a rectangular two-dimensional column were carried out to study the rise characteristics of single bubbles, bubble-bubble interactions and coalescence-breakup phenomena.

Our experiments show that the hydrodynamics is significantly affected by column diameter, elevated system pressures, concentration of the slurry. These effects are not adequately described by published literature correlations.

The extrapolation of data obtained in laboratory cold flow units to the commercial scale reactors requires a systematic approach based on the understanding of the scaling principles of bubble dynamics and of the behaviour of two-phase dispersions in large scale columns.

We develop a multi-tiered approach to bubble column reactor scale-up, relying on a combination of experiments, backed by Computational Fluid Dynamics (CFD) simulations for physical understanding. This approach consists of the following steps:

– *description of single bubble morphology and rise dynamics; here both experiments and Volume of Fluid (VOF) simulations are used;*
– *modelling of bubble-bubble interactions;*
– *description of the behaviour of bubble swarms and of the development of the proper interfacial momentum exchange relations between the bubbles and the liquid;*
– *CFD simulations in the Eulerian framework for extrapolation of laboratory scale information to large scale commercial reactors.*

Keywords: Fischer-Tropsch synthesis, bubble column slurry reactor, flow regimes, scale-up strategy, holdup, mixing, mass transfer, modelling.

NOTATION

AF	wake acceleration factor, dimensionless
B	constant in Reilly correlation
c	concentration of ethanol in water, vol%
C_D	drag coefficient, dimensionless
d_b	diameter of either bubble population, m
d_p	particle size, m
$D_{ax,\,L}$	liquid phase axial dispersion coefficient, m^2/s
DF	density correction factor, dimensionless
$Đ_L$	diffusion coefficient in the liquid phase, m^2/s
$Đ_{L,\,ref}$	reference diffusion coefficient in the liquid, m^2/s
D_T	column diameter, m
Eö	Eötvös number, $g(\rho_L - \rho_G)d_b^2/\sigma$
g	acceleration due to gravity, 9.81 m/s^2
H	dispersion height of the reactor, m
k_La	volumetric mass transfer coefficient, s^{-1}
M	Morton number, $g\mu_L^4(\rho_L - \rho_G)\rho_L^2/\sigma^3$
n	Richardson-Zaki index, dimensionless
p	pressure, Pa or bar
r	radial coordinate, m
Re	Reynolds number, $\rho_L d_b V_b/\mu_L$
SF	scale correction factor, dimensionless
T	reactor temperature, K
U	superficial gas velocity, m/s
$(U - U_{df})$	superficial gas velocity through the large bubbles, m/s
U_{df}	superficial velocity of gas through the small bubbles, m/s
$V_{b,\,small}$	rise velocity of the small bubbles, m/s
$V_{b,\,small,\,0}$	rise velocity of the small bubbles at 0% solids concentration, m/s
$V_{b,\,large}$	rise velocity of the large bubbles, m/s
$V_L(r)$	radial distribution of liquid velocity, m/s
$V_L(0)$	centre-line liquid velocity, m/s
U_{df}	superficial gas velocity through the "dense" phase, m/s
U_{trans}	superficial gas velocity at regime transition, m/s
z	axial coordinate, m

Greek Letters

α, β	parameters defined by Equation (9)
α_{ASF}	Anderson-Schulz-Flory chain growth probability factor, dimensionless
ε	total gas holdup, dimensionless
ε_b	gas holdup of large bubbles, dimensionless
ε_{df}	gas holdup of the "dense phase", dimensionless
ε_s	volume fraction of catalyst in the slurry phase, dimensionless
ε_{trans}	gas holdup at the regime transition point, dimensionless
μ_L	liquid viscosity, Pa·s
ν	kinematic viscosity of phase, m^2/s
ρ_G	density of gas phase, kg/m^3
$\rho_{G,\,ref}$	density of gas phase at atmospheric conditions, kg/m^3
ρ_L	liquid density, kg/m^3
σ	surface tension of liquid phase, N/m

Subscripts

b	referring to large bubble phase
CO	referring to CO species
df	referring to small bubbles
G	referring to gas phase
H	referring to H_2
L	referring to liquid phase
large	referring to large bubbles
p	referring to solid particles
s	referring to solids
SL	referring to slurry
small	referring to small bubbles
trans	referring to regime transition point
T	tower or column

INTRODUCTION

The Fischer-Tropsch reaction that was discovered in Germany nearly three quarters of a century ago has recently become a subject of renewed interest, particularly in the context of the conversion of remote natural gas to liquid transportation fuels. The main incentives for this conversion are the increased availability of natural gas in remote locations for which no nearby markets exist, and the growing demand for middle distillate transportation fuels (gasoil and kerosine) especially in the Pacific and Asian regions. Natural gas can be converted to carbon monoxide and hydrogen (synthesis gas) *via* existing or newly developed processes such as steam reforming, carbon dioxide reforming, partial oxidation and catalytic partial oxidation, followed by the Fischer-Tropsch synthesis reaction:

$$CO + 2\,H_2 \rightarrow "–CH_2–" + H_2O + 170\ kJ \qquad (1)$$

in which "$–CH_2$" represents a product consisting mainly of paraffinic hydrocarbons of variable chain length. In most cases, the chain length distribution of the product follows an Anderson-Schulz-Flory distribution function characterised by a chain growth probability factor α_{ASF}.

For economic and logistic reasons, such energy conversions are best carried out in large scale projects and the

capability of upscaling is therefore an important consideration in the selection of reactors for synthesis gas generation as well as in Fischer-Tropsch synthesis. Another important issue in Fischer-Tropsch synthesis is the strong exothermicity: *e.g.*, compared to processes applied in the oil industry, the heat released per unit weight of feed or product is an order of magnitude higher and corresponds with a theoretical adiabatic temperature rise of about 1600 K at complete conversion. Unless the product is so light that it is completely vaporised under reaction conditions, the reaction takes place in a three-phase system: gas (carbon monoxide, hydrogen, steam and gaseous hydrocarbon products), liquid product and solid catalyst. The amounts of syngas and product molecules that have to be transferred between the phases are quite large: *i.e.*, an order of magnitude larger than the amount of hydrogen molecules to be transferred in hydroprocessing of oils. Therefore, great demands are placed on the effectiveness of interfacial mass transfer in Fischer-Tropsch synthesis.

A careful examination of the published literature [1-6] shows that the viable reactor choices for a commercial process aimed at the production of relatively heavy hydrocarbon products are the multi-tubular fixed bed operating in the trickle flow regime *(Fig. 1)* and the bubble column slurry reactor *(Fig. 2)*. These two reactor types can be built with substantially higher capacities (2500 bbl/d or higher) than the reactors developed before, during and shortly after World War II. The maximum feasible capacity is not fixed; however, as other factors besides the fundamental limitations discussed so far can play a role. Aside from mechanical construction aspects, the weight of the reactor can be a limiting factor if the reactor has to be transported and erected in remote areas with poorly developed infrastructure. For offshore installation on fixed and floating platforms, other limiting criteria such as floor space needed and maximum height may apply.

For a specific case of conversion of syngas into a relatively heavy Fischer-Tropsch product, De Swart *et al.* [6] have compared the multi-tubular trickle-bed reactor with slurry reactors operating in either the homogeneous or the heterogeneous regime. With a maximum weight of 900 t per reactor as limiting criterion, the number of reactors needed for a plant capacity of 5000 t/d (approx. 40 000 bbl/d) were found to be 10 for the multi-tubular trickle bed, 17 for the slurry reactor operating in the homogeneous regime, and 4 for the bubble column slurry reactor operating in the heterogeneous flow regime.

While the maximum achievable capacity in Fischer-Tropsch reactors is undoubtedly a very important factor in the economy of large scale natural gas conversion, it is not the only one that governs reactor choice. Reactor costs may differ for different reactors of equal capacity, depending upon the complexity of construction. In this regard too, the slurry bubble column may compare favourably with the multi-tubular fixed bed. Catalyst loading and unloading in bubble column slurry reactors is much easier than in multi-tubular fixed bed reactors and can be accomplished in a shorter time. Moreover, the activity of the catalyst inventory in the reactor can be maintained by withdrawal of catalyst and replacement with fresh catalyst during a run. In the case of the synthesis of heavy Fischer-Tropsch products, separation of solids from the liquid in the slurry reactor technology may not be a trivial problem. Distilling off the product is not possible with heavy liquids, and filtering may prove necessary. The separation problem is aggravated if fines are produced by catalyst attrition (either mechanical or chemical attrition). It is necessary to avoid attrition of catalyst in slurry reactor operation.

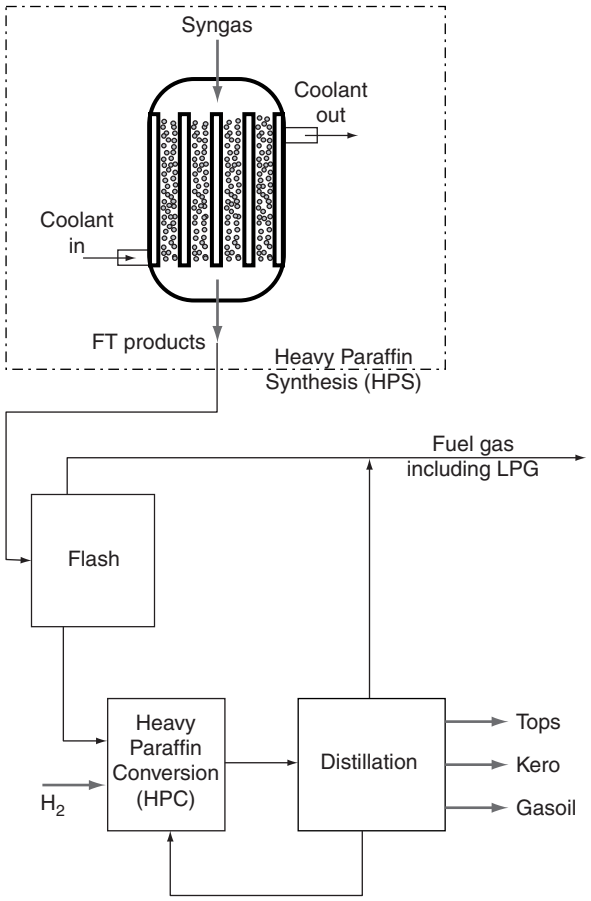

Figure 1

Schematic of the SMDS process, which involves heavy paraffin synthesis, followed by hydrocracking of the paraffins to produce products predominantly in the diesel range. A multi-tubular trickle bed reactor is used in the Fischer-Tropsch synthesis step. For process description see [5].

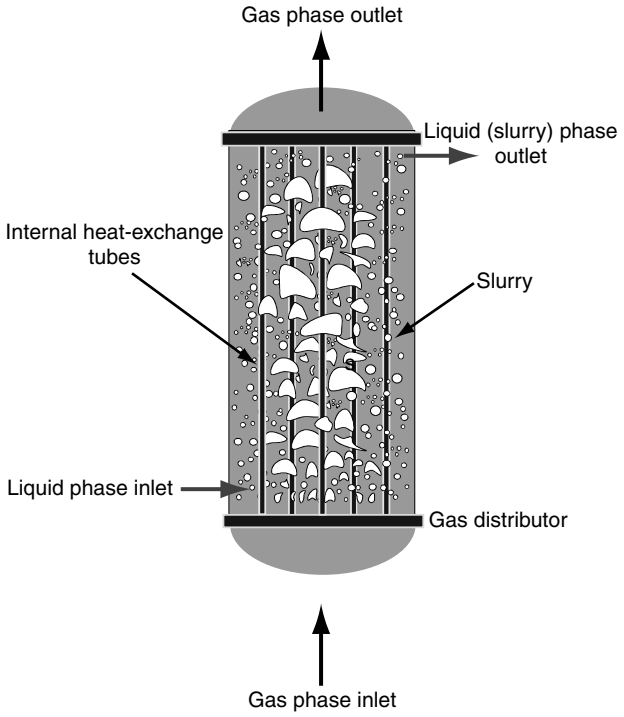

Figure 2

The bubble column slurry reactor configuration with internal cooling.

In view of the foregoing arguments, we believe that the bubble column slurry reactor is the best choice of reactor type for large scale plants with capacities of the order of 40 000 bbl/d. Typical design and operating conditions of a Fischer-Tropsch slurry bubble column diameter for an optimally designed reactor are given below:

- the column diameter ranges from 6 to 10 m;
- the column height is in the range 30-40 m;
- the reactor operates at a pressure of between 3-5 Mpa;
- the reactor temperature is about 513-523 K;
- the superficial gas velocity is in the range 0.2-0.4 m/s depending on the catalyst activity and the catalyst concentration in the slurry phase;
- for high reactor productivities, the highest slurry concentrations consistent with catalyst handleability should be used. In practice the volume fraction of catalyst in the slurry phase, ε_s, is in the range 0.3-0.4;
- for removing the heat of reaction 5000-8000 vertical cooling tubes, say of 50 mm diameter and 150 mm pitch, will need to be installed in the reactor.

The success of the process largely depends on the ability to achieve deep syngas conversions, approaching 90% or higher. Reliable design of the reactor to achieve such high conversion levels requires reasonable accurate information on the following hydrodynamic and mass transfer parameters:

- gas holdup;
- interphase mass transfer between the gas bubbles and the slurry;
- axial dispersion of the liquid (slurry) phase;
- heat transfer coefficient to cooling tubes.

The correlations and models available in standard texts on bubble column reactors [7, 8] fall outside the scope of conditions relevant for the Fischer-Tropsch process. In this review we try to develop procedures for estimating the required information, using more recently available experimental data, largely generated at the University of Amsterdam [9-38].

1 GAS HOLDUP IN BUBBLE COLUMNS

1.1 Hydrodynamic Regimes

When a column filled with a liquid is sparged with gas the bed of liquid begins to expand as soon as gas is introduced. As the gas velocity is increased the bed height increases almost linearly with the superficial gas velocity U, provided the value of U stays below a certain value U_{trans}. This regime of operation of a bubble column is called the *homogeneous bubbly flow regime*. The bubble size distribution is narrow and a roughly uniform bubble size, generally in the range 1-7 mm, is found. When the superficial gas velocity U reaches the value U_{trans}, coalescence of the bubbles takes place to produce the first fast-rising "large" bubble. The appearance of the first large bubble changes the hydrodynamic picture dramatically. The hydrodynamic picture in a gas-liquid system for velocities exceeding U_{trans} is commonly referred to as the *heterogeneous* or *churn-turbulent flow regime* [9, 12, 15, 17, 19]. In the heterogeneous regime, small bubbles combine in clusters to form large bubbles in the size range 20-70 mm [14, 18]. These large bubbles travel up through the column at high velocities (in the range 1-2 m/s), in a more or less plug flow manner [19, 28]. These large bubbles have the effect of churning up the liquid phase [17, 33]. The large bubbles are mainly responsible for the throughput of gas through the reactor [17]. Small bubbles, which co-exist with large bubbles in the churn-turbulent regime, are "entrained" in the liquid phase and as a good approximation have the same backmixing characteristics of the liquid phase [17]. The two regimes are portrayed in Figure 3 which shows also in a qualitative way the variation of the gas holdup ε as a function of the superficial gas velocity U. When the gas distribution is very good, the regime transition region is often characterised by a maximum in the gas holdup [11]. The transition between homogeneous and churn-turbulent regimes is often difficult to characterise.

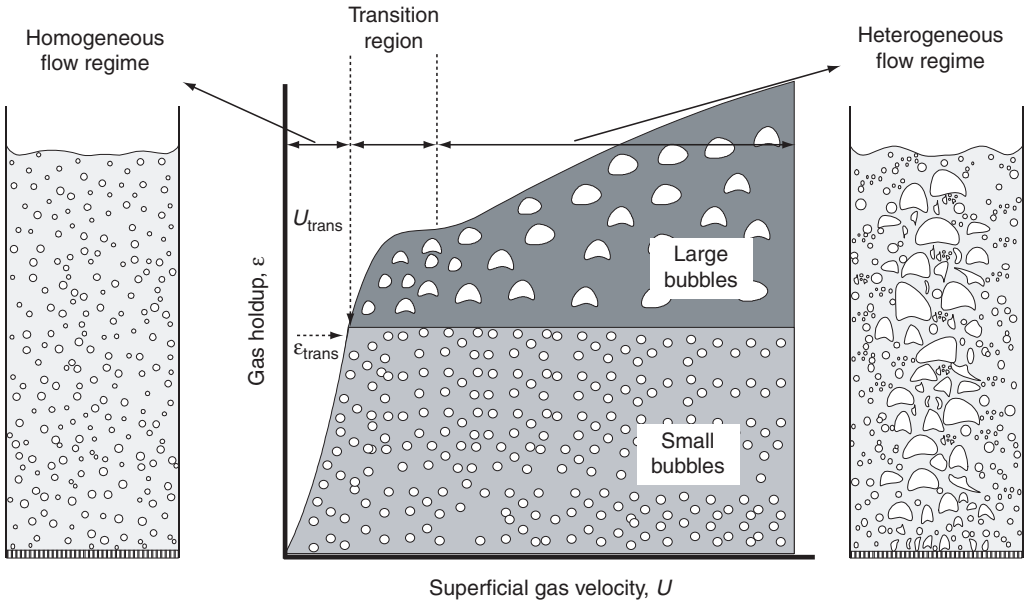

Figure 3

Homogeneous and churn-turbulent regimes in a gas-liquid bubble column.

1.2 The Problems of Estimating the Gas Holdup

The estimation of the gas holdup in the bubble column slurry reactor for Fischer-Tropsch synthesis is an important but an extremely difficult task.

The gas holdup varies significantly with liquid properties; see data in Figure 4 for air-paraffin oil (ρ_L = 795 kg/m^3; μ_L = 0.0029 Pa·s; σ = 0.029 N/m), air-water (ρ_L = 1000; μ_L = 0.001; σ = 0.072) and air-Tellus oil (ρ_L = 862; μ_L = 0.075; σ = 0.028) measured in a column of 0.38 m diameter with a sintered plate distributor. *The gas holdup appears to also depend on the column diameter;* see data in Figure 5 for air-paraffin oil, air-water and air-Tellus oil measured in columns of 0.1 and 0.38 m diameter, both with a sintered plate distributor. *Literature correlations for the gas holdup in bubble columns show a wide spread* in their capabilities to predict the variation with respect to U and with respect to the column diameter D_T. Figure 6a compares air-water experimental data in a 0.38 m diameter column as a function of U with several literature correlations [39-45]. Only the Krishna-Ellenberger [19] correlation matches the data successfully, but this is to be expected because their correlation was developed including the data set shown! Figure 6b compares air-water gas holdup predictions from different correlations as a function of column diameter for a constant superficial gas velocity U = 0.2 m/s. Only two correlations, those of Zehner [45] and Krishna and Ellenberger [19], predict a decline in ε with increasing column diameter DT. It should not be forgotten that for the Fischer-Tropsch process we need to extrapolate to column diameters of 6 to 10 m! Figures 7a and 7b present the corresponding information for air-Tellus oil; here we note that most literature correlations perform even worse than for the air-water system.

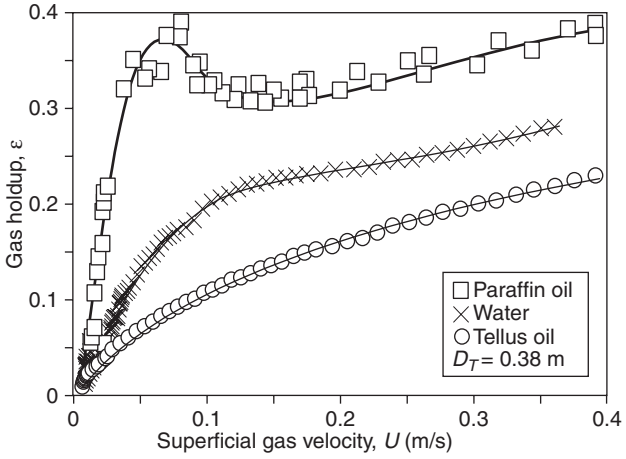

Figure 4

Comparison of the total gas holdup measured in a column of 0.38 m internal diameter. Measurements with air-paraffin oil, air-water and air-Tellus oil.

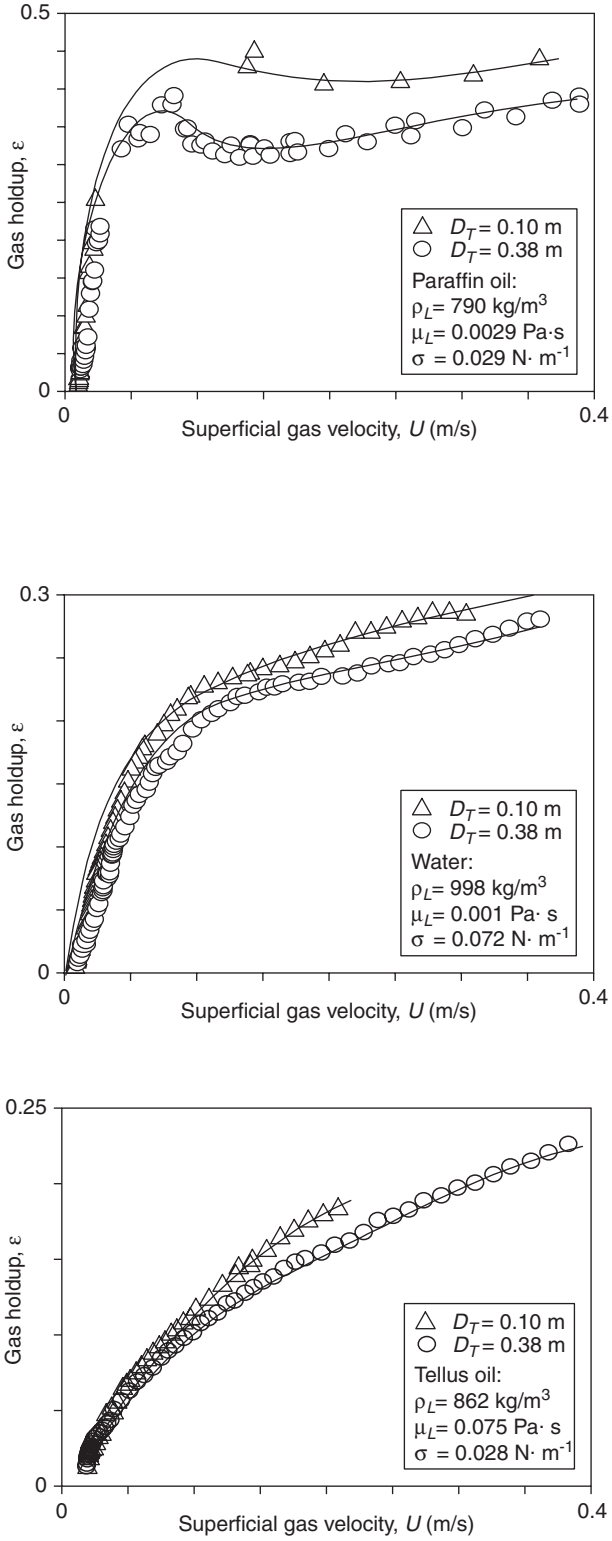

Figure 5

Comparison of the total gas holdup measured in columns of 0.1 and 0.38 m internal diameter. Measurements with air-paraffin oil, air-water and air-Tellus oil.

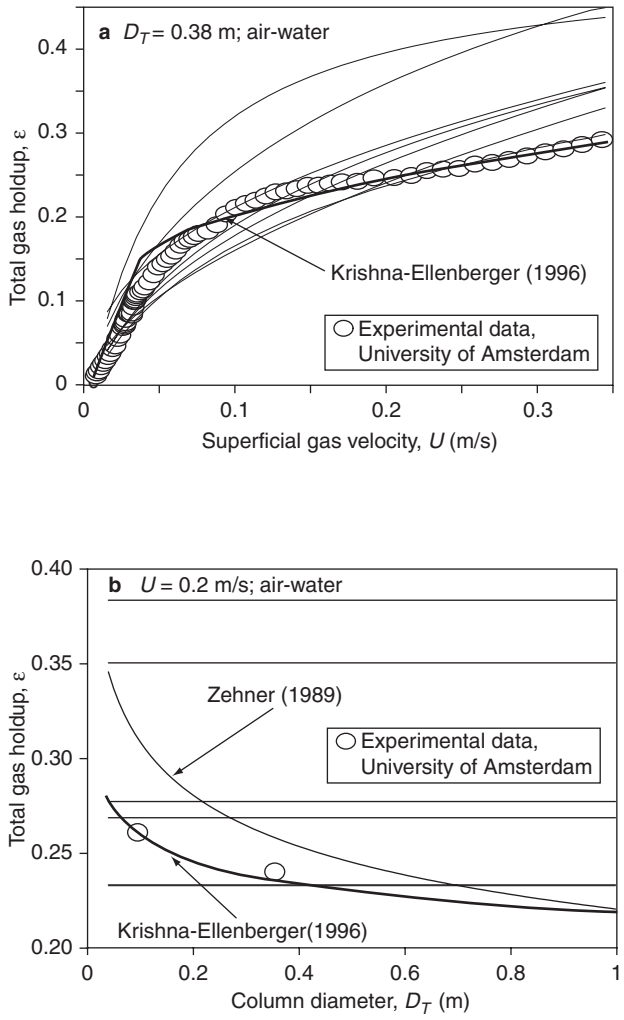

Figure 6

Comparison of literature correlations and experimental data for the total gas holdup ε for air-water system in a column of 0.38 m diameter.

(a) Variation of ε with superficial gas velocity for a column of 0.38 m diameter.

(b) Variation of ε with column diameter for a superficial gas velocity of 0.2 m/s.

The plotted correlations are to be found in [19, 39-45].

Clearly, we need a proper understanding of bubble hydrodynamics, as a function of scale (column diameter and height) and physical properties of gas and liquid phases before we could develop reliable procedures for scaling up a Fischer-Tropsch slurry reactor. So we start with trying to understand the behaviour of single gas bubbles in a liquid.

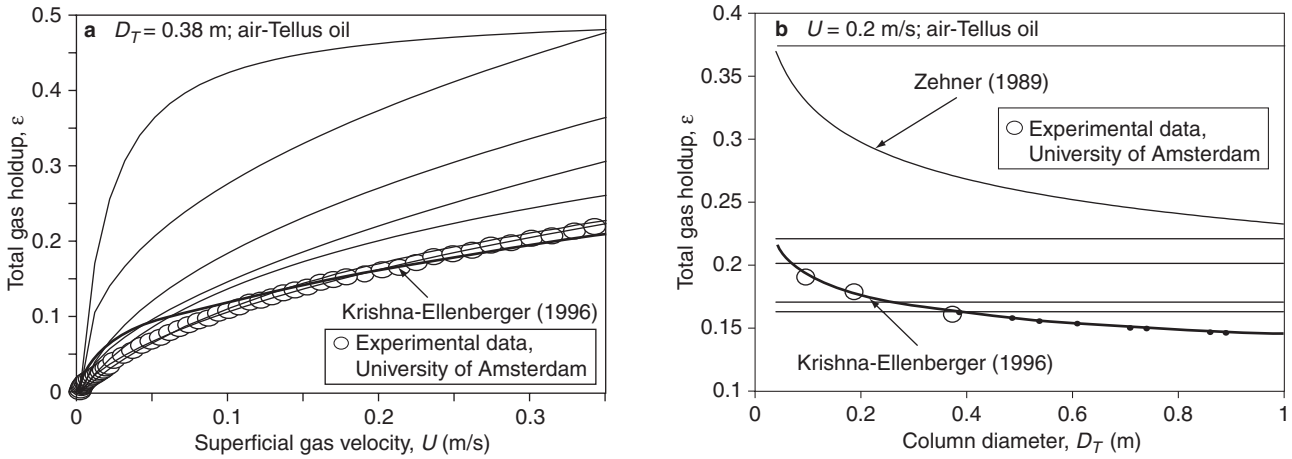

Figure 7

Comparison of literature corrrelations and experimental data for the total gas holdup ε for air-Tellus oil system in a column of 0.38 m diameter.

(a) Variation of ε with superficial gas velocity for a column of 0.38 m diameter.

(b) Variation of ε with column diameter for a superficial gas velocity of 0.2 m/s.

Same correlations as specified in the legend to Figure 6.

1.3 The Rise Characteristics of Single Gas Bubbles in a Liquid

The morphology and rise characteristics of a bubble are strongly dependent on the bubble size and system properties. A generalised graphical representation [46, 47] of the rise characteristics is given in Figure 8 in terms of three dimensionless groups:

– Eötvös number, $\text{Eö} \equiv \dfrac{g(\rho_L - \rho_G)d_b^2}{\sigma}$

– Morton number, $\text{M} \equiv \dfrac{g\mu_L^4(\rho_L - \rho_G)}{\rho_L^2\sigma^3}$

– Reynolds number, $\text{Re} \equiv \dfrac{\rho_L d_b V_b^0}{\mu_L}$

where d_b is the bubble diameter, taken to be equal to the diameter of a sphere with the same volume as that of the actual bubble and V_b^0 is the rise velocity of a single, isolated bubble. For the system air-water, M = 2.63×10^{-11}, log(M) = –10.6, we note that when increasing the bubble size from say 4 (corresponding to Eö = 2.2) to 20 mm (Eö = 54.4) the regime changes from "wobbling" to "spherical cap". Using Computational Fluid Dynamics (CFD) and the Volume of Fluid (VOF) techniques, Krishna and Van Baten [29] have unravelled the rich dynamic features of air bubbles rising in a column of water *(Fig. 9)*. The 4 and 5 mm bubbles show meandering trajectories. The 7 mm bubble oscillates

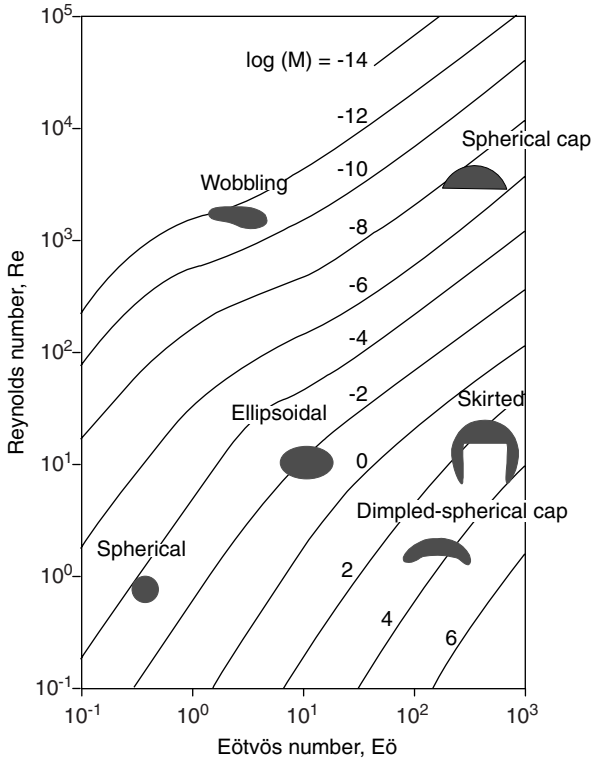

Figure 8

Shape regimes for bubble rising in a column of liquid. Adapted from [46].

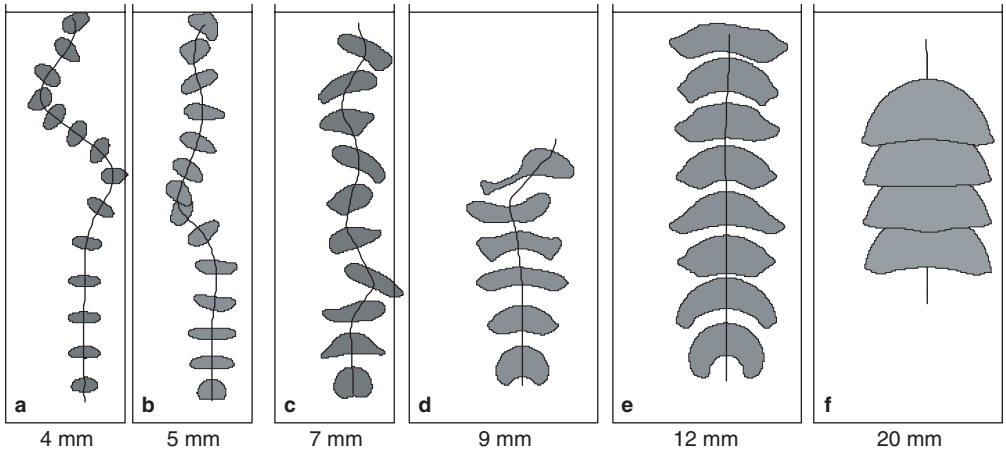

Figure 9

Snapshots obtained with two-dimensional VOF simulations of the rise trajectories of bubbles in the 4-12 mm size range.
(a) Snapshots of 4 mm bubble at times t = 0.0415, 0.0955, 0.1495, 0.2035, 0.2575, 0.3115, 0.3655, 0.4195, 0.4735, 0.5275, 0.5815, 0.6355 and 0.6895 s from the start of the simulations.
(b) Snapshots of 5 mm bubble at times t = 0.0285, 0.0825, 0.1365, 0.1905, 0.2445, 0.2985, 0.3525, 0.4065, 0.4605, 0.5145, 0.5685, 0.6225, 0.6765 and 0.7305 s.
(c) Snapshots of 7 mm bubble at times t = 0.0285, 0.1005, 0.1725, 0.2445, 0.3165, 0.3885, 0.4605, 0.5325, 0.6045 and 0.6765 s.
(d) Snapshots of 9 mm bubble at times t = 0.0415, 0.1135, 0.1855, 0.2575, 0.3295 and 0.4015 s.
(e) Snapshots of 12 mm bubble at times t = 0.0595, 0.1315, 0.2035, 0.2755, 0.3475, 0.4195, 0.4915 and 0.5635 s.
(f) Snapshots of 20 mm bubble at times t = 0.1675, 0.2395, 0.3115 and 0.3835 s.
Animations of all these VOF simulations can be viewed on our web site (http://ct-cr4.chem.uva.nl/single_bubble).

from side to side when moving up the column. The 9 mm bubble behaves like jellyfish. The 12 mm bubble flaps its "wings" like a bird. The 20 mm bubble assumes a spherical cap shape and has a vertical rise trajectory. These rich dynamic features can be viewed by looking at the animations on our web site (http://ct-cr4.chem.uva.nl/single_bubble/). As the bubble size increases, the amplitude of the excursions in the x-directions decreases *(Fig. 10)*.

In general, the bubble rise velocity of single gas bubbles is affected by scale because of "wall effects". The magnitude of the wall effects depends on the ratio of the bubble diameter to the column diameter, d_b/D_T. When the column diameter is large enough, the bubbles are free from wall effects. Figure 11 shows measured rise velocities of air bubbles of varying sizes in a column of 0.63 m diameter, which can be considered large enough for wall effects not to play a role. The bubble rise velocity can be described reasonably accurately by the Mendelson [48] equation:

$$V_b^0 = \sqrt{\frac{2\sigma}{\rho_L d_b} + \frac{g d_b}{2}} \tag{2}$$

where the superscript 0 is used to emphasise the fact that we are considering the rise velocity of a single, isolated bubble. For values of Eö > 40 (for air-water system, this corresponds to bubble sizes larger than 17 mm), Equation (2) simplifies to give the classic Davies and Taylor [49] relationship for spherical cap bubbles:

$$V_b^0 = \sqrt{\frac{g d_b}{2}} = 0.71\sqrt{g d_b} \tag{3}$$

The relationship (3) is remarkable in that the rise velocity does not depend on the physical properties of either the liquid or gas. The Davies-Taylor relationship (3) is found applicable, provided the ratio $d_b/D_T < 0.125$. For values of d_b/D_T exceeding 0.125, Collins [50] introduced a scale correction factor, SF, into the Davies-Taylor relationship:

$$V_b^0 = 0.71\sqrt{g d_b}\ (SF) \tag{4}$$

This scale correction factor was determined empirically to be given by Collins [50] as follows:

$$\begin{aligned} SF &= 1 && \text{for } \frac{d_b}{D_T} < 0.125 \\ SF &= 1.13\exp\left(-\frac{d_b}{D_T}\right) && \text{for } 0.125 < \frac{d_b}{D_T} < 0.6 \\ SF &= 0.496\sqrt{\frac{D_T}{d_b}} && \text{for } \frac{d_b}{D_T} > 0.6 \end{aligned} \tag{5}$$

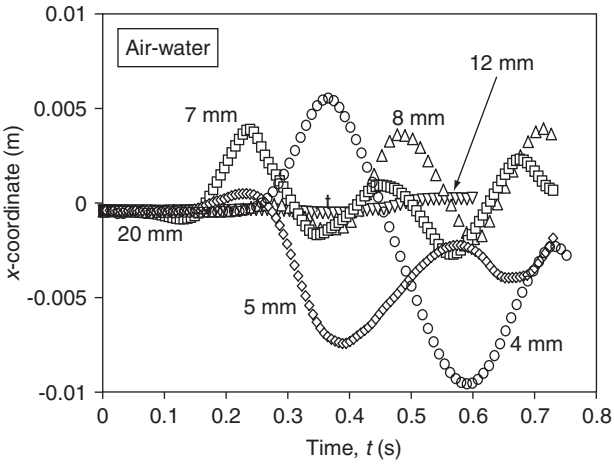

Figure 10

Comparison of the x-trajectories obtained with two-dimensional VOF simulations of bubbles in the 4-20 mm size range.

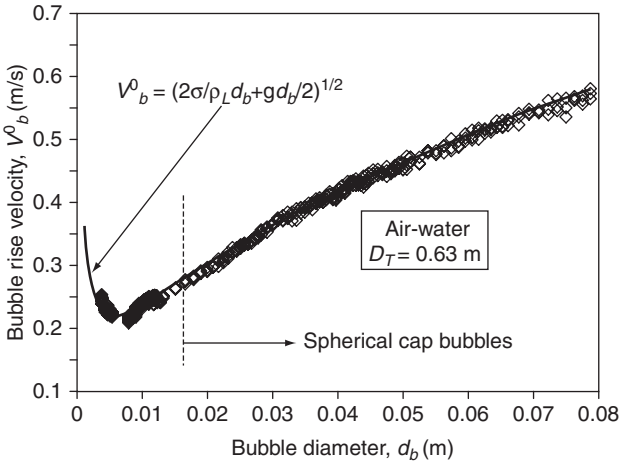

Figure 11

Rise velocity of air bubbles of varying diameters in a 0.63 m diameter column filled with water; comparison of experimental data with the predictions of the Mendelson equation (2).

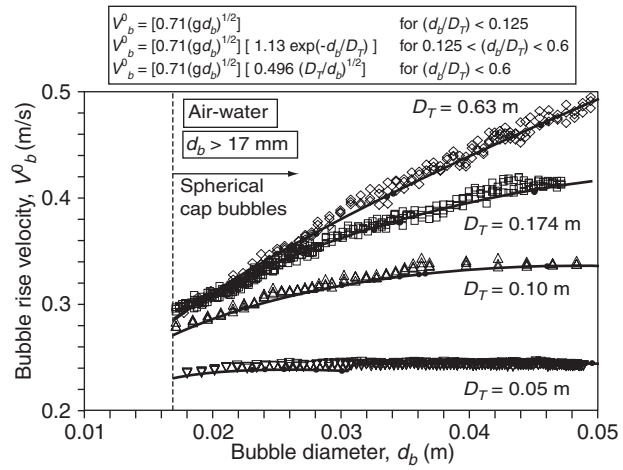

Figure 12

Rise velocity of air bubbles of varying diameters in columns of 0.051, 0.1, 0.174 and 0.63 m diameter filled with water; comparison of experimental data with the predictions of the Davies-Taylor-Collins equations (4) and (5).

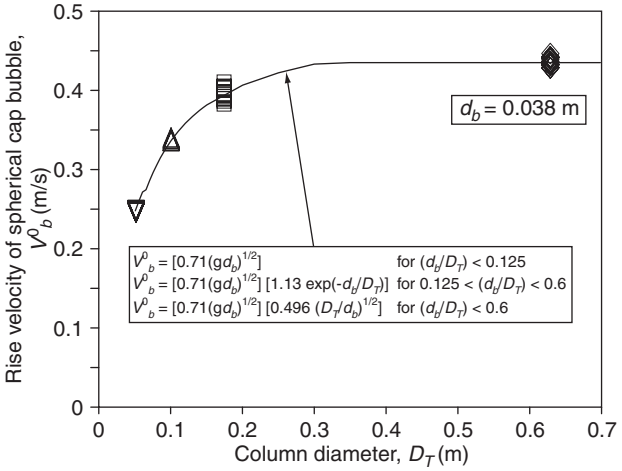

Figure 13

Influence of column diameter on the rise velocity of an air bubble of 0.038 m diameter in water. Comparison of experimental data with the predictions of the Davies-Taylor-Collins equations (4) and (5).

The conditions wherein $d_b/D_T > 0.6$ correspond to the special case of slug flow for which the bubble rise velocity is independent of the bubble diameter and is given by:

$$V_b^0 = 0.35\sqrt{gD_T} \qquad (6)$$

Extensive experiments carried out at the University of Amsterdam in four different columns of diameter 0.051, 0.1, 0.174 and 0.63 m with the air-water system confirm the validity of the Davies-Taylor-Collins relations (4) and (5) *(Fig. 12)*. The strong influence of the scale factor on the rise velocity is emphasised when we consider the rise of a bubble of 0.038 m diameter as a function of column diameter *(Fig. 13)*. In the 0.051 m diameter column we have slugging *(cf. Eq. (6))* and the rise velocity is 0.25 m/s. For the 0.1 m diameter column the rise velocity is 0.34 m/s, rising to 0.44 m/s in the 0.63 m diameter column. In order to give a

physical understanding of the wall effects, we compare in Figure 14 the z-coordinates of the nose of 21 mm bubbles rising in columns of 0.1 and 0.051 m diameter filled with water obtained from VOF simulations. Figure 14 shows that the bubble rises faster in the wider column. The reason for this is the restraining effect of the walls. The insets to Figure 14 show the liquid phase velocity profiles for these two simulations. We notice that the 21 mm bubble assumes a flatter shape in the 0.1 m wide column and is less influenced by the wall than the same bubble placed in a 0.051 m wide column. Put another way, the drag between the bubble and the liquid is higher in the column of smaller width due to the higher downward liquid velocity in the vicinity of the bubble. The VOF simulations yield values of the rise velocity which are in excellent agreement with measured experimental data *(Fig. 15)*.

For the 0.1 m diameter column, rise velocities of air bubbles were measured in highly viscous Tellus oil which has a viscosity 75 times that of water; the results, shown in Figure 16, confirm the fact that the rise velocity is independent of the physical properties of the liquid. We will see later that this is an important conclusion for the Fischer-Tropsch slurry reactor.

The prediction of the rise characteristics of bubbles smaller than say 17 mm, corresponding to Eö < 40, is not an easy task because of the rich dynamic features, which are also particularly sensitive to system properties and presence of impurities, etc. Clift *et al*. [46] and Fan and Tsuchiya [47] give detailed procedures for the estimation of the rise velocities for this "regime". Wall effects are also important for bubbles smaller than 17 mm; these effects can be again described by introducing another scale factor into the Mendelson equation:

$$V_b^0 = \sqrt{\frac{2\sigma}{\rho_L d_b} + \frac{g d_b}{2}}\,(SF)$$
$$SF = \left[1 - \left(\frac{d_b}{D_T}\right)^2\right]^{\frac{3}{2}} \tag{7}$$

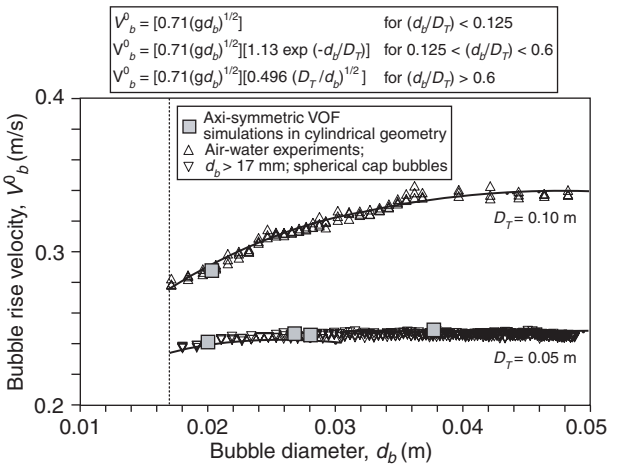

Figure 15

Rise velocity of air bubbles of varying diameters in columns of 0.051 and 0.1 m diameter filled with water. Comparison of experimental data with the predictions of the Davies-Taylor-Collins equations (4) and (5) and VOF simulations.

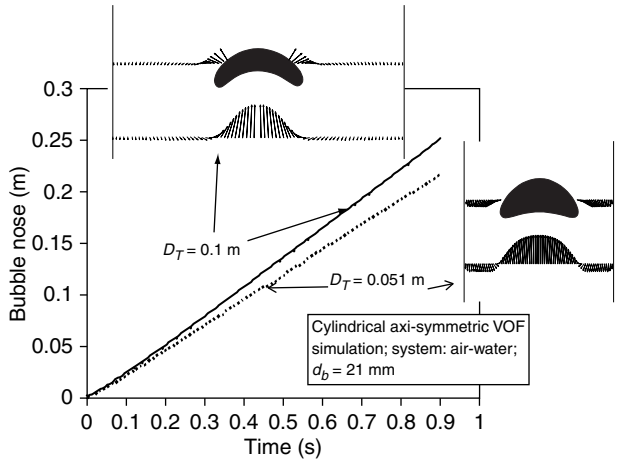

Figure 14

VOF simulations of the rise trajectories of a 21 mm diameter bubble in 0.051 and 0.1 m diameter columns. The insets show the liquid phase velocity profiles surrounding the bubble.

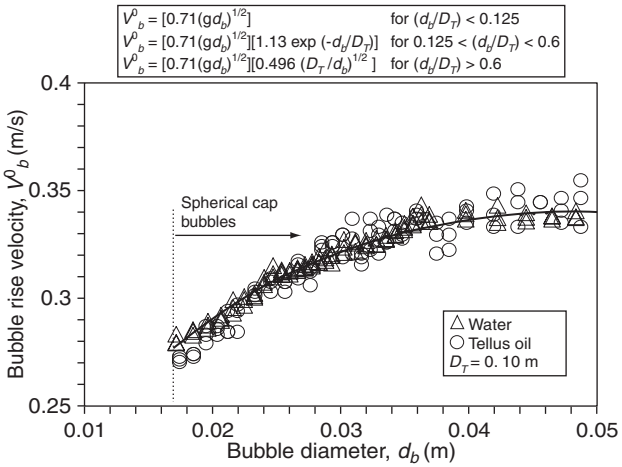

Figure 16

Rise velocity of air bubbles of varying diameters in a 0.1 m diameter column filled with water and Tellus oil. Comparison of experimental data with the predictions of the Davies-Taylor-Collins equations (4) and (5).

The validity of Equation (7), suggested by Clift *et al.* [46], has been confirmed by extensive air-water experiments *(Fig. 17)*. In practice the scale correction factor for bubbles smaller than 17 mm is not significant even for laboratory-sized columns say of 0.1 m diameter.

Summarising, we recommend use of Equations (4) and (5) for Eö > 40 and of Equation (7) for Eö < 40. In further discussions on the subject of bubble columns we shall be talking about "small" and "large" bubbles. Roughly speaking, "small" bubbles are taken to represent bubbles smaller than about 17 mm; "large" bubbles are taken to correspond to the requirement of Eö > 40, corresponding to sizes larger than about 17 mm. It is important to distinguish between these bubble classes because "small" bubbles have morphologies and rise characteristics which are significantly affected by system properties. "Large" bubbles, on the other hand, are relatively insensitive to system properties. The rise characteristics of large bubbles are however significantly affected by scale.

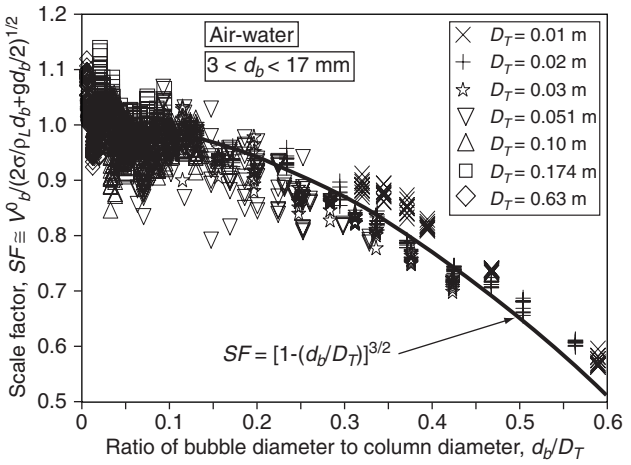

Figure 17

Influence of scale on the rise velocity of bubbles smaller than 17 mm. Test of the modified Mendelson equation (3) with experimental data for the bubble size range of 3-17 mm.

1.4 Behaviour of Swarms of "Small" Bubbles

Let us first consider the homogeneous regime of operation in which we have a swarm of "small" bubbles, typically smaller than about 5 mm in size. A single small bubble in this size range exhibits lateral movement as shown in Figures 9 and 10. The behaviour of a swarm of such bubbles is interesting because the lateral motion of each bubble affects the neighbouring bubble. The resulting swarm motion is best appreciated by viewing VOF simulations of a swarm of 5 mm bubbles in a column of water (see our web site http://ct-cr4.chem.uva.nl/single_bubble/). Snapshots of these simulations are shown in Figure 18. Each bubble in the swarm tends to "avoid" each other. This "avoidance" can also be viewed as mutual "hindering" of the rise velocity. In the chemical engineering literature, the hindered rise of gas bubbles is described by the Richardson-Zaki [51] relation:

$$V_b = V_b^0 (1-\varepsilon)^{n-1} \tag{8}$$

where the bubble swarm velocity V_b^0 is obtained by "correcting" the single bubble rise velocity V_b^0 for the finite gas holdup of the gas bubbles ε. The exponent n is the Richardson-Zaki index and for air bubbles in water has a value of about 2, *i.e.* $n \approx 2$. As the gas holdup ε increases, the bubble swarm velocity decreases. For a gas holdup ε = 0.1, the decrease in the bubble swarm velocity is about 10% when compared to the single bubble value V_b^0.

1.5 Behaviour of Swarms of "Large" Bubbles

Before building up an understanding of the swarms of "large" bubbles, let us consider the interactions between "large" bubble pairs. Figure 19a shows the retraced pictures of video recordings of the rise of two 47 mm diameter bubbles in a 0.63 m diameter column when their starting vertical positions are at the same horizontal plane. The horizontal distance of separation of these two bubbles is 0.12 m. The two bubbles rise at the same velocity, corresponding to the value they would have were they to be injected individually. Their rise velocities are not affected by each other. However, when the starting vertical positions of these two 47 mm bubbles are slightly different (0.07 m vertical separation), the trailing bubble quickly gets sucked into the wake of the leading bubble and during this process it experiences an accelerated rise *(Fig. 19b)*. Note that the trailing bubble gets vertically aligned with the leading bubble before coalescence occurs. Figure 19c shows another experiment in which the initial position of two bubbles, of 40 and 50 mm size, are horizontally aligned. As expected, the 50 mm bubble rises faster and accelerates the smaller bubble until coalescence takes place. Note again that the smaller 40 mm trailing bubble aligns itself vertically behind the leading bubble before coalescence occurs.

In order to quantify the acceleration effect experienced by the trailing bubble, let us consider two bubbles of the same size, d_b = 31 mm, separated vertically in a 0.051 m diameter column *(Fig. 20)*. It is clear that the acceleration effect increases as the trailing bubble approaches the leading bubble. The VOF simulation of this experiment is shown in Figure 21. The reason why the shape of the bubbles in the VOF simulations appears to be hollower than in the

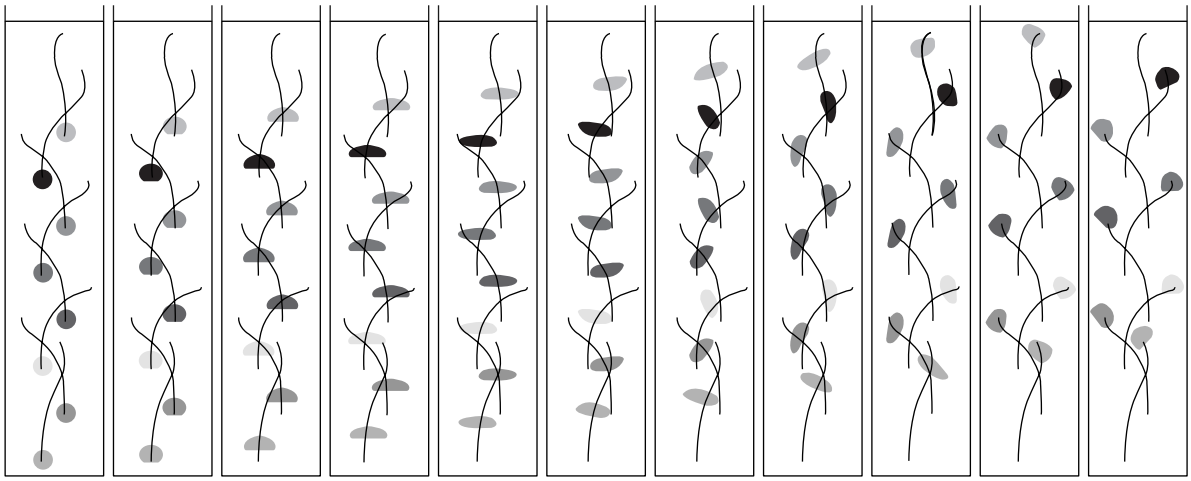

Figure 18

Rise trajectories of a swarm of 5 mm bubbles, eight in number, in a column of water. Animations of all these VOF simulations can be viewed on our web site (http://ct-cr4.chem.uva.nl/single_bubble).

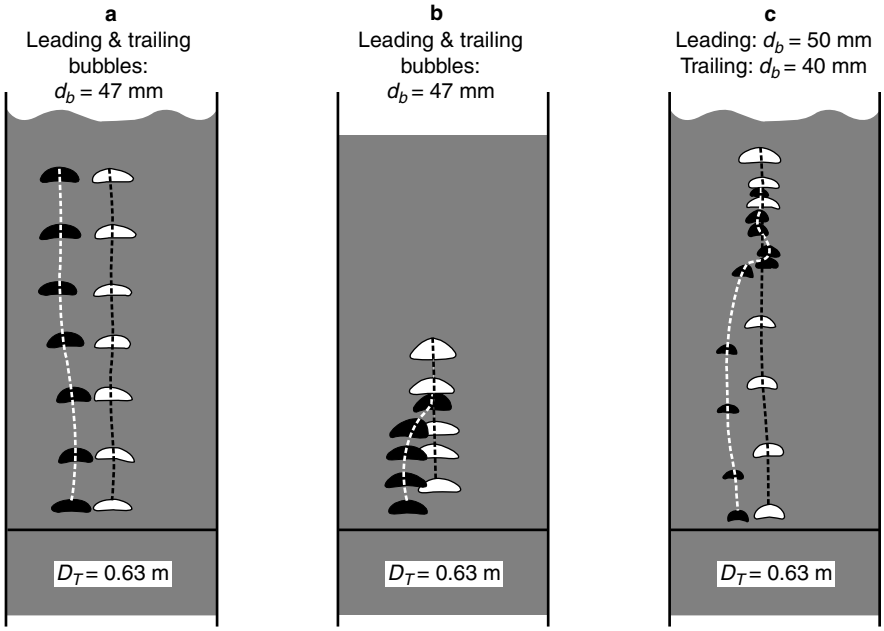

Figure 19

(a) Rise trajectories of two 47 mm diameter bubbles in water, separated by a horizontal distance of 0.12 m. Both bubbles are released simultaneously. Column diameter is 0.63 m.

(b) Rise trajectories of two 47 mm diameter bubbles in water, separated by 0.1 m horizontally. Initial vertical separation is 0.07 m between the two bubbles.

(c) Rise trajectories of two bubbles in water, 40 and 50 mm in diameter, separated by 0.1 m horizontally. Both bubbles are released simultaneously.

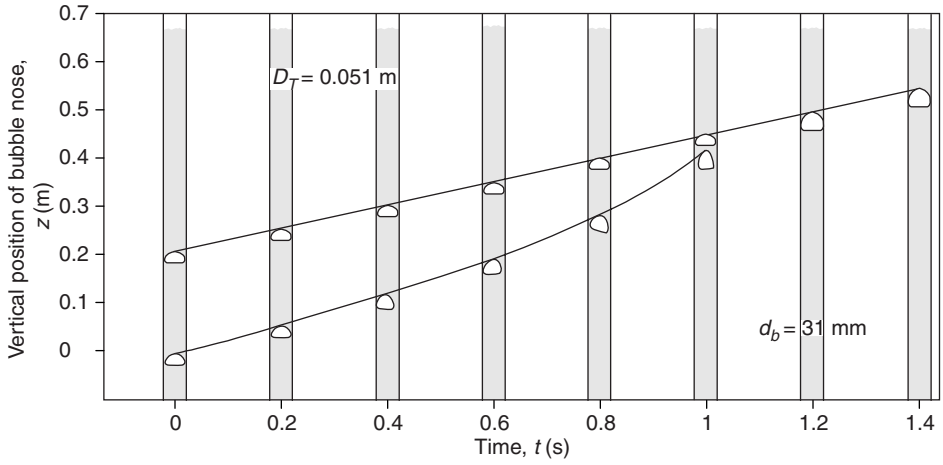

Figure 20

Retraced video images of in-line interactions of 31 mm diameter bubbles rising in a 0.051 m diameter column filled with water.

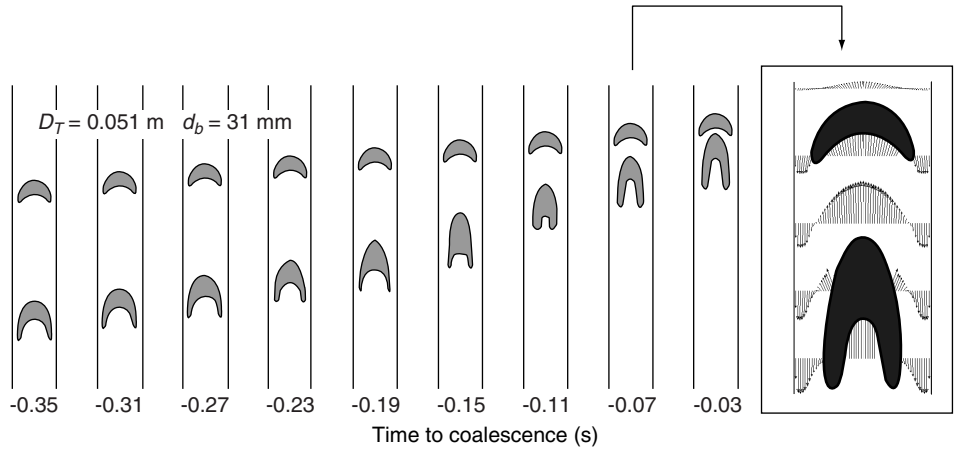

Figure 21

VOF simulations, using cylindrical axi-symmetry, of the experiment shown in Figure 20. The inset shows the liquid phase velocity profiles for the situation corresponding to 0.07 s before coalescence. Animations of this VOF simulation can be viewed on our web site (http://ct-cr4.chem.uva.nl/axissym).

experiment is due to the fact that in the video recordings only the outer periphery of the bubbles can be visualised. The contours of the bubbles in Figure 21, on the other hand, are drawn for a slice in the *r-z* plane. The liquid phase velocity profiles at 0.07 s before coalescence of the bubbles are indicated in the inset in Figure 21. The trailing bubble is sucked into the wake of the leading bubble. Animations of the VOF simulations performed to study in-line interactions of bubbles in various liquids can be viewed on our web site (http://ct-cr4.chem.uva.nl/axissym). A comparison of the

measured trajectories for both leading and trailing bubbles with VOF simulations shows very good agreement *(Fig. 22)*.

The slope of the rise trajectory at any instant of time yields the rise velocity. We define an acceleration factor, *AF*, for the trailing bubble as the ratio of the actual velocity to the velocity it would have were the same bubble uninfluenced by other bubbles; this latter velocity can be obtained from Equations (4) and (5). In Figure 23, the experimentally observed acceleration factor for the trailing bubble is plotted against its distance of separation Δz from the leading bubble. The acceleration factor *AF* is seen to increase as Δz decreases in a more or less linear fashion. For a given separation distance, the value of *AF* decreases with increasing liquid viscosity. For example, when Δz = 0.05 m, the value of *AF* for water is about 3. This means that the trailing bubble travels upwards with a velocity which is three times higher than V_b^0, given by Equations (4) and (5).

Similar measurements to that shown in Figure 20, performed with highly viscous Tellus oil (μ_L = 0.075), gives acceleration factors which are significantly lower *(Fig. 23)*. When Δz = 0.05 m, the value of *AF* for Tellus oil is about 2.5. The wake interaction effects are weaker in highly viscous liquids. The wake interaction effects in "low" viscosity liquids (say with μ_L < 0.003 Pa·s) can be expected to be of comparable magnitude.

The acceleration factor *AF* determined from experiments shown in Figure 23 is valid for a bubbling trailing another bubble. We need to extend this concept to a swarm of "large" bubbles in a bubble column operating in the churn-turbulent regime. For this purpose we first consider a simplified picture of the hydrodynamics in this regime, put forward by Krishna and Ellenberger [19] *(Fig. 24)*. The dispersion is assumed to consist of two bubble classes: small and large. The superficial gas velocity through the small bubble population is assumed to be equal to that at the regime transition point U_{trans}. The remainder of the entering gas flows up the column in the form of large bubbles. The superficial gas velocity through the large bubble "phase" is therefore $(U - U_{trans})$. For steady-state mode of operation in the churn-turbulent regime, every "large" bubble is a "trailing" bubble because there will be a bubble preceding it. The large bubble swarm velocity can therefore be expected to be much higher than that of a single, isolated bubble, V_b^0. From the foregoing discussion we should expect the acceleration factor *AF* to increase linearly with decreasing distance of separation of the bubbles. With increasing values of $(U - U_{trans})$ we should expect the average distance of separation between the large bubbles to decrease. We therefore assert that:

$$V_b = V_b^0(AF)$$
$$AF = \alpha + \beta(U - U_{trans}) \quad (9)$$

where V_b^0 is given by Equations (4) and (5). The experimental data on the large bubble swarm velocity V_b as a function

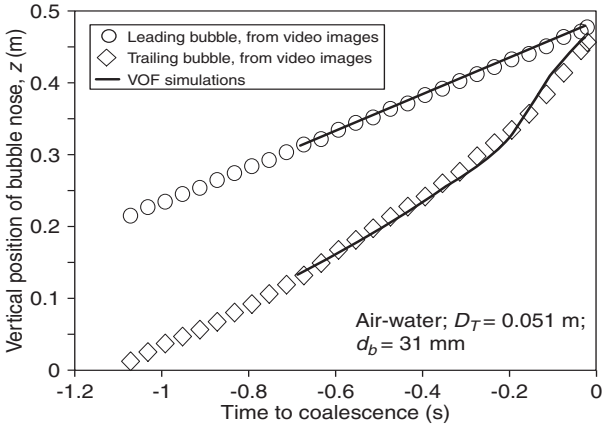

Figure 22

Comparison between experiment and VOF simulations of the rise trajectories of the leading and trailing bubbles in a 0.051 m diameter column filled with water.

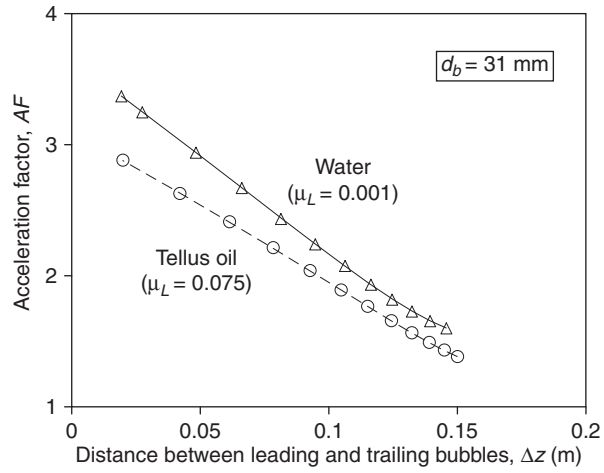

Figure 23

The acceleration factor for the trailing bubble as function of its distance of separation from the preceding bubble. The measurements with Tellus oil were made in a 0.1 m diameter column and those with water were made in a 0.051 m diameter column.

of $(U - U_{trans})$ reported in Krishna and Ellenberger [19] comprised of more than 1000 measured points with liquids of relatively low viscosity (less than 0.0029 Pa·s) were used to obtain the following expressions for the average large bubble diameter:

$$d_b = 0.069(U - U_{trans})^{0.376} \quad (10)$$

and the acceleration factor, *AF*:

$$AF = 2.73 + 4.505\,(U - U_{trans}) \text{ (low viscosity liquids)} \quad (11)$$

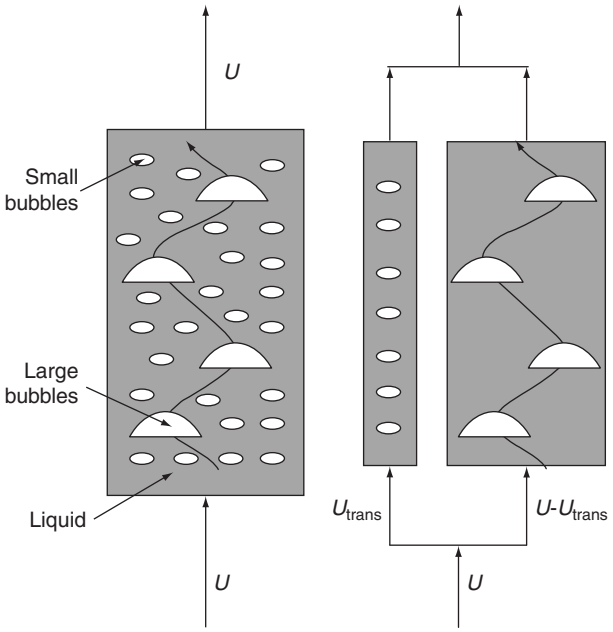

Figure 24

Three-phase model for bubble columns operating in the churn-turbulent regime.

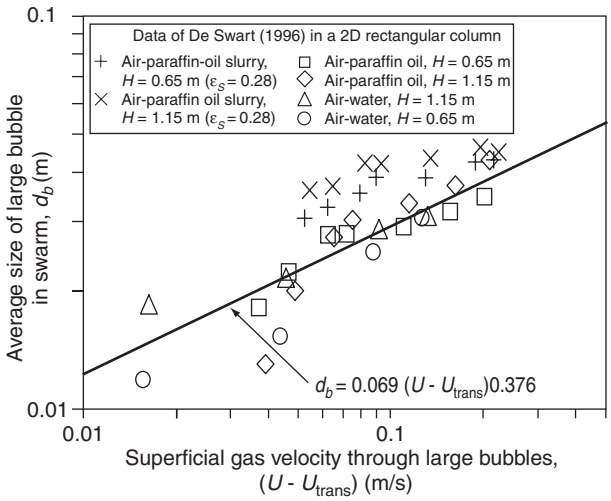

Figure 25

Correlation for the average bubble size of large bubble swarm as function of the superficial gas velocity through the large bubble population. The experimental data is to be found in [18] measured with the systems air-water, air-paraffin oil and air-paraffin oil slurry (28 vol% solids) in a 2D rectangular column of 0.3 m width at different heights H above the distributor.

The fitted bubble size correlation (10) matches very well with the measured bubble size data of De Swart *et al.* [18] in a two-dimensional rectangular bubble column *(Fig. 25)*. In Figure 26 we compare the experimental values of the large bubble swarm velocity V_b for the air-water system measured in three different columns with the predictions of Equations (4), (5), (9)-(11).

From the large bubble swarm velocity measurements made with the system air-Tellus oil [28], the corresponding fit for the acceleration factor is:

$$AF = 2.25 + 4.09\,(U - U_{\text{trans}}) \quad \text{(Tellus oil)} \qquad (12)$$

while the fit for the bubble size d_b remains the same as for "low" viscosity liquids, *i.e.* Equation (10). From Figure 25 it is interesting to note that the bubble size relationship (10) also gives a reasonable estimation of the bubble size in concentrated slurries. Figure 27 testifies to the goodness of the fit of the data for the swarm velocity of large bubbles in Tellus oil.

In order to demonstrate the importance of scale, and of bubble-bubble interaction leading to acceleration of the rise velocity, let us consider a bubble column operating at $(U - U_{\text{trans}}) = 0.2$ m/s. The bubble size d_b can be calculated from Equation (10) to be 0.038 m. The single bubble rise velocity and the large bubble swarm velocities for air-water and air-Tellus oil systems can be calculated from Equations (4), (5), (9)-(12) as a function of column diameter D_T; the results are shown in Figure 28. It is interesting to note that while the single bubble rise velocity in water and Tellus oil are the same, the bubble swarm velocity is higher in water. The wake effects are more important in low viscosity liquids.

1.6 A Model for Total Gas Holdup

In the foregoing section we have developed models for determining the rise velocity of small and large gas bubble swarms in liquids, including the influence of system properties and scale. In this section we develop a model for estimating the total gas holdup.

For superficial gas velocities, $U < U_{\text{trans}}$, we have homogeneous bubbly flow and only "small" bubbles are present in the system. In this regime the total gas holdup can be calculated from:

$$\varepsilon = \frac{U}{V_{b,\text{small}}} \qquad U < U_{\text{trans}} \qquad (13)$$

(homogeneous bubbly flow)

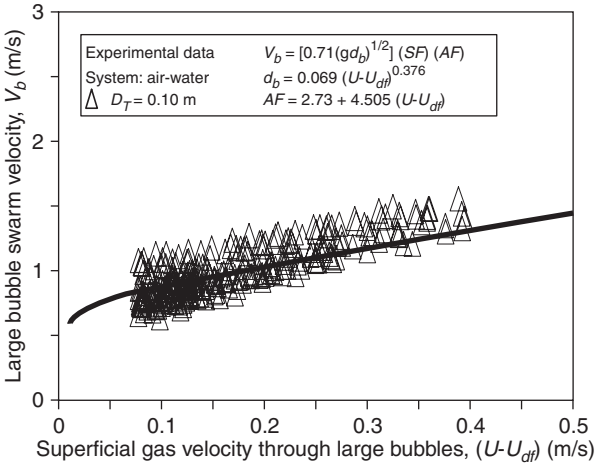

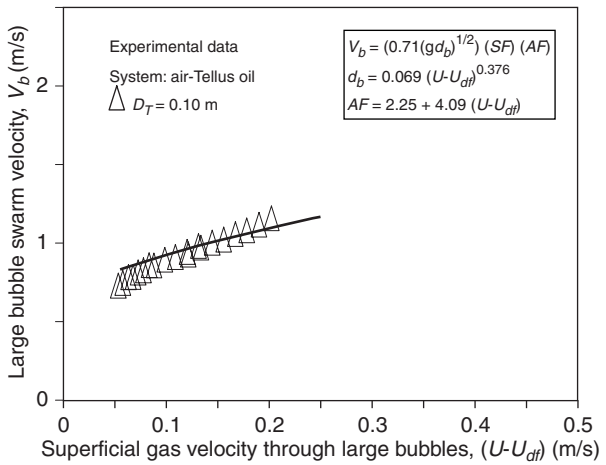

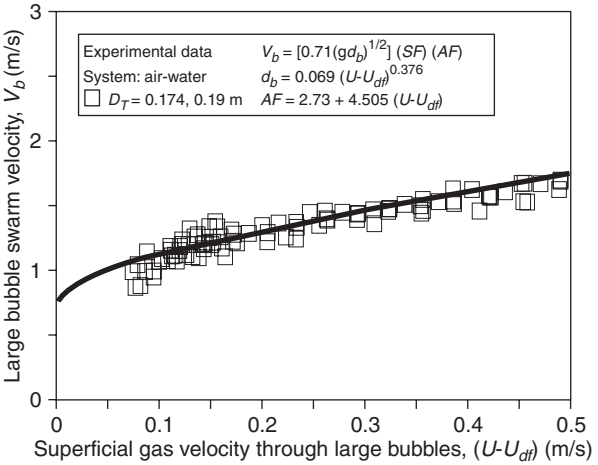

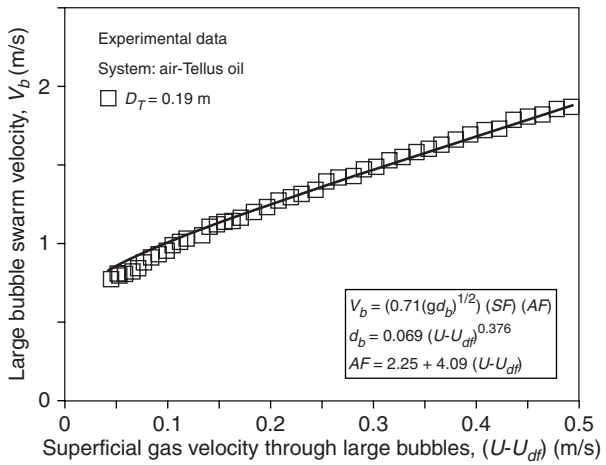

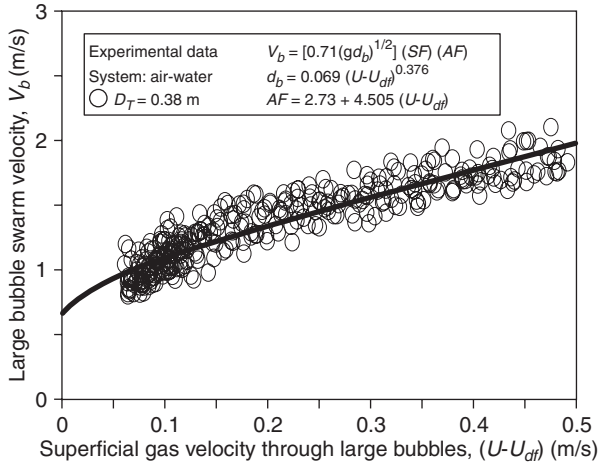

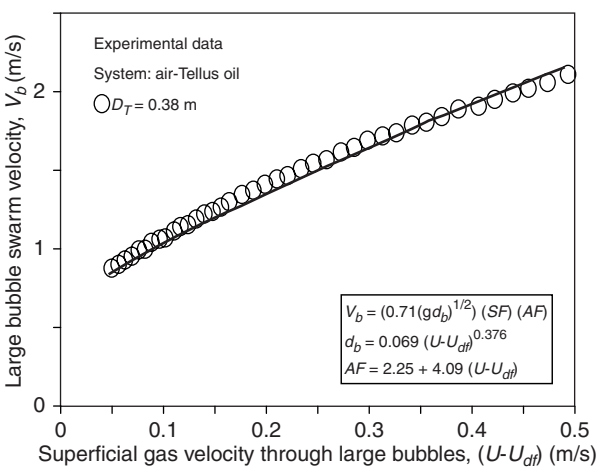

Figure 26

Rise velocity of large bubble swarms in water measured in columns of 0.1, 0.174 and 0.38 m diameter. The rise velocity was determined by the dynamic gas disengagement technique. Comparison of experimental data with the estimations using Equations (4), (5), (9)-(11).

Figure 27

Rise velocity of large bubble swarms in Tellus oil measured in columns of 0.1, 0.19 and 0.38 m diameter. The rise velocity was determined by the dynamic gas disengagement technique. Comparison of experimental data with the estimations using Equations (4), (5), (9), (10) and (12).

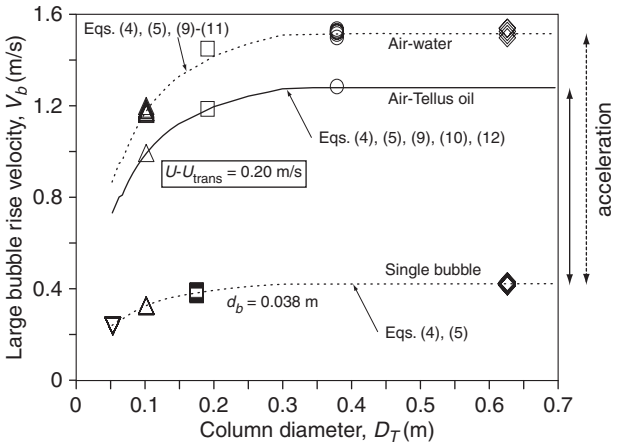

Figure 28

Influence of column diameter on the rise velocity of large bubble swarm, with an average diameter of 0.038 m, obtained at $(U - U_{trans}) = 0.2$ m/s.

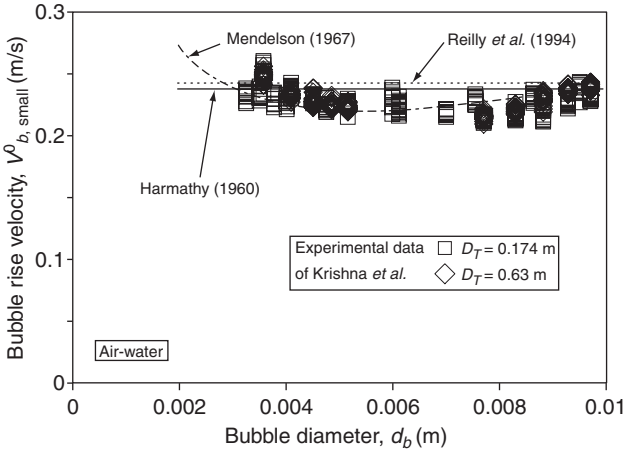

Figure 29

Influence of bubble diameter on the rise velocity of small bubbles in water. Comparison of experimental data with the correlations found in [48, 52, 53].

where the small bubble swarm velocity $V_{b,\,small}$ is obtained by correcting the single bubble velocity V_b^0, small for the hindering effect *(cf. Eq. (8))*:

$$V_{b,\,small} = V^0_{b,\,small}(1 - \varepsilon) \tag{14}$$

where we take the Richardson-Zaki exponent $n = 2$. There are several correlations for calculating the single bubble rise velocity, for example due to Harmathy [52]:

$$V^0_{b,small} = 1.53\left(\frac{\sigma g}{\rho_L}\right)^{0.25} \tag{15}$$

and Reilly *et al*. [53]:

$$V^0_{b,small} = \frac{1}{2.84}\frac{1}{\rho_G^{0.04}}\sigma^{0.12} \tag{16}$$

Figure 29 compares measured single bubble rise velocity of bubbles smaller than 0.01 m with the correlations of Harmathy [52], Mendelson [48] and Reilly *et al*. [53]. All three correlations appear to be in reasonable agreement with experiment. Combining Equations (13) and (14) we obtain:

$$\varepsilon = \frac{U}{V^0_{b,small}(1-\varepsilon)} \qquad U < U_{trans} \tag{17}$$

(homogeneous bubbly flow)

and so an iterative procedure is required to determine the gas holdup.

Homogeneous bubbly flow prevails up to the regime transition velocity, U_{trans}. This parameter is difficult to estimate, and the only correlation that appears to be reasonable is that of Reilly *et al*. [53]:

$$U_{trans} = V^0_{b,small}\varepsilon_{trans}(1-\varepsilon_{trans})$$
$$\varepsilon_{trans} = 0.59B^{1.5}\sqrt{\frac{\rho_G^{0.96}}{\rho_L}\sigma^{0.12}} \tag{18}$$

where ε_{trans} is the gas holdup at the regime transition point. The parameter $B = 3.85$.

For operation in the heterogeneous or churn-turbulent flow regime, the total gas holdup is made up of two contributions: due to small bubbles and due to large bubbles. Due to the large recirculatory flow which is present in the heterogeneous flow regime the small bubbles are intimately mixed with the liquid, and in the hydrodynamic picture of Krishna and Ellenberger [19] a pseudo-phase, called the "dense" phase, is defined, which consists of small bubbles dispersed in the liquid *(Fig. 30)*. The fractional gas holdup within this dense phase is denoted by ε_{df}. The parameter ε_{df} has been determined by dynamic gas disengagement experiments to be practically independent of the superficial gas velocity. A good estimation of the dense phase gas holdup is given by the gas holdup at regime transition:

$$\varepsilon_{df} \approx \varepsilon_{trans} \tag{19}$$

The superficial gas velocity through the "dense" phase U_{df} can also be approximated as follows:

$$U_{df} \approx U_{trans} \tag{20}$$

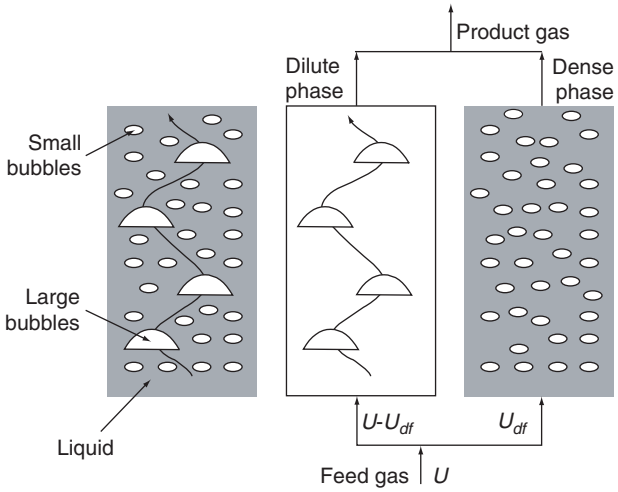

Figure 30

The two-phase model of a bubble column reactor operating in the churn-turbulent flow regime. Definition of "dilute" and "dense" phases.

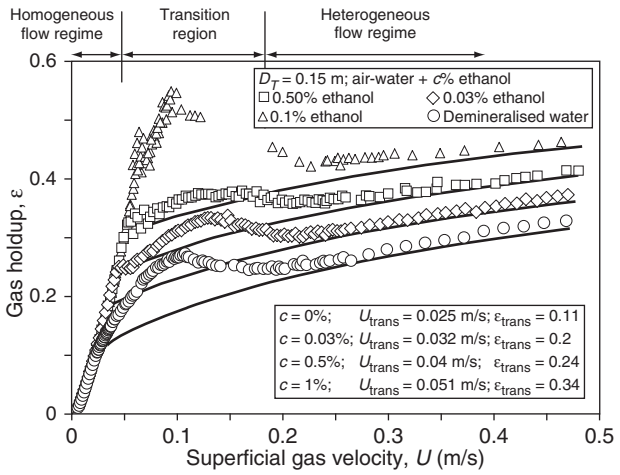

Figure 31

Experimental data showing the influence of ethanol addition in varying concentrations to water on gas holdup. Comparison of experimental data from [30] with the estimations using Equations (4), (5), (9)-(11).

The gas holdup of the large bubbles, also called the "dilute" phase, can be estimated from:

$$\varepsilon_{b,\,\mathrm{large}} = \frac{U - U_{df}}{V_{b,\,\mathrm{large}}} \tag{21}$$

where $V_{b,\,\mathrm{large}}$, the large bubble swarm velocity, is to be estimated for low viscosity liquids from Equations (4), (5), (9)-(11) and for high viscosity liquids we use Equation (12) in place of Equation (11) to acceleration factor. The total gas holdup in the heterogeneous flow regime is calculated from:

$$\varepsilon = \varepsilon_{b,\,\mathrm{large}} + (1 - \varepsilon_{b,\,\mathrm{large}})\varepsilon_{df} \qquad U > U_{\mathrm{trans}} \tag{22}$$

The transition gas velocity, U_{trans}, is extremely sensitive to addition of small amounts of surface active agents and this effect is not encompassed in Equation (18) of Reilly *et al.* [53]. It is best to determine U_{trans} experimentally. To illustrate this, in Figure 31, we present experimental data on the total gas holdup obtained in a 0.15 m diameter column with water, 0.03 and 0.5% ethanol in water solution. The experimental data is compared with the theoretical predictions using Equations (17), (19)-(22) with experimentally determined values of U_{trans}. The agreement of the model in the heterogeneous flow regime is excellent. For the transition regime there is no adequate model to predict the total gas holdup. The important point to conclude from the results presented in Figure 31 is that a shift in the regime transition point, U_{trans}, to the right causes a significant increase in the gas holdup in the heterogeneous regime. This increase is purely to be ascribed to the increase in the gas holdup at the regime transition point, $\varepsilon_{\mathrm{trans}}$.

1.7 Influence of Elevated Pressure on the Gas Holdup in Bubble Columns

Elevated pressure operation has a significant influence on the gas holdup as is evidenced by the experimental results of Letzel *et al.* [21, 31] for gas holdup measured in a bubble column of 0.15 m diameter with the system nitrogen-water *(Fig. 32)*. For example, for operation at a superficial gas velocity U = 0.2 m/s, the gas holdup ε can increase from a value of 0.29 at p = 0.1 MPa to a value which is twice as large for operation at p = 1.2 MPa. Increased system pressure influences:

- the regime transition point, U_{trans};
- the gas voidage at the regime transition point, $\varepsilon_{\mathrm{trans}}$;
- the large bubble holdup, $\varepsilon_{b,\,\mathrm{large}}$.

We discuss these, in turn, below.

Several workers [10, 11, 21, 32, 44, 53] have shown that with increased system pressure the gas holdup at the transition point, $\varepsilon_{\mathrm{trans}}$, increases. The correlation of Reilly *et al.* [53], Equation (18), is adequate for estimation purposes. In the Reilly correlation, the influence of system pressure is captured in the gas density, ρ_G. The "small" bubble rise velocity, $V^0_{b,\,\mathrm{small}}$, is only very weakly dependent on the gas density. The superficial gas velocity through the dense phase,

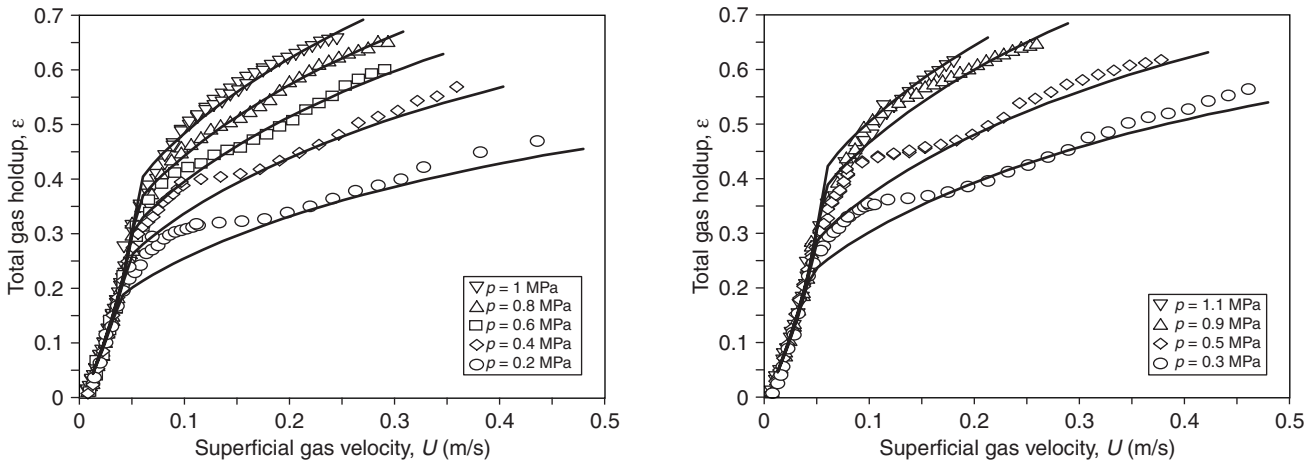

Figure 32

Influence of increased system pressure on gas holdup. Experimental data found in [31] compared with model predictions using Equations (4), (5), (9)-(11), (23) and (24).

$U_{df} = U_{\text{trans}} = V^0_{b,\text{ small}}\varepsilon_{\text{trans}}(1 - \varepsilon_{\text{trans}})$ increases significantly with increasing gas density.

A more recently published effect of elevated pressure is that the large bubbles become less stable [25]. To account for this, we introduce a further gas density correction factor, *DF*, into Equations (4) and (9):

$$V_{b,\text{ large}} = 0.71\sqrt{gd_b}\,(SF)(AF)(DF) \tag{23}$$

Using the Kelvin-Helmholtz stability theory as basis, Letzel *et al*. [25] concluded that *DF* is inversely proportional to the square root of the gas density. For air at atmospheric conditions used in the experiments, $\rho_G = 1.29$ kg/m^3 and the density correction factor is unity, *i.e*. $DF = 1$. For any gas at any system pressure, having a gas density ρ_G, the density correction factor can be calculated from:

$$DF = \sqrt{\frac{1.29}{\rho_G}} \tag{24}$$

The Fischer-Tropsch synthesis of hydrocarbons in a bubble column slurry reactor is carried out at a pressure of about 30 MPa. The syngas density at this pressure is 7 kg/m^3 and the large bubble rise velocity at these conditions is only a fraction $\sqrt{1.29/7} = 0.43$ of the velocity it would have in cold flow experiments carried out under atmospheric pressure conditions with air as the gas phase. This underlines the importance of the density correction factor developed above.

The modification given by Equations (23) and (24) can be introduced into Equations (17)-(22) for estimation of the total holdup in bubble columns operated at elevated pressures. The estimations using this procedure are compared with experimental data in Figure 32. The agreement between model predictions and experiment is remarkably good, especially considering no experimental data inputs were used in the estimations.

1.8 Influence of Catalyst Addition on the Hydrodynamics

The same picture as shown in Figure 3 holds for a bubble column slurry reactor when fine catalyst particles (typically smaller than 50 μm) are used [16, 18, 20, 26]. The fine catalyst particles are intimately mixed with the liquid and the slurry phase can be considered pseudo-homogeneous. The assumption of a pseudo-homogeneous slurry phase, where no catalyst settling takes place, is a good one for operation of large diameter columns (say larger than 0.5 m) at high superficial gas velocities ($U > 0.2$ m/s).

When the concentration of solid particles (catalyst) in the liquid increases, the total gas holdup ε is reduced. Furthermore, the transition to the heterogeneous flow regime occurs at a lower superficial gas velocity [20, 32]. The data for paraffin oil slurries to which solid particles have been added illustrates this effect [20] *(Fig. 33)*. The properties of paraffin oil are $\rho_L = 795$ kg/m^3, $\mu_L = 0.0029$ Pa·s and $\sigma = 0.029$ N/m. The solid phase used consisted of porous silica particles whose properties were determined to be as follows:

- skeleton density = 2100 kg·m^{-3};
- pore volume = 1.05 mL·g^{-1};
- particle size distribution, d_p: 10% < 27 μm; 50% < 38 μm; 90% < 47 μm.

The solids concentration ε_s is expressed as the volume fraction of solids in gas free slurry. The pore volume of the particles (liquid filled during operation) is counted as being

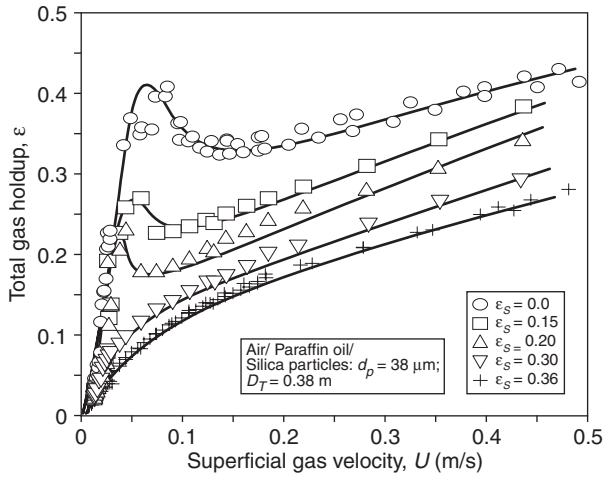

Figure 33

Influence of increased particles concentration on the total gas holdup in a 0.38 m diameter column. The experimental data is from [20]. Air was used as the gas phase in all experiments. The liquid phase was paraffin oil (density, ρ_L = 790 kg·m^{-3}; viscosity, μ_L = 0.0029 Pa·s; surface tension, σ = 0.028 N·m^{-1}) to which solid particles in varying concentrations were added. The solid phase used consisted of porous silica particles (skeleton density = 2100 kg·m^{-3}; pore volume = 1.05 mL·g^{-1}; particle size distribution, d_p: 10% < 27 μm; 50% < 38 μm; 90% < 47 μm). The solids concentration ε_s is expressed as the volume fraction of solids in gas free slurry. The pore volume of the particles (liquid filled during operation) is counted as being part of the solid phase.

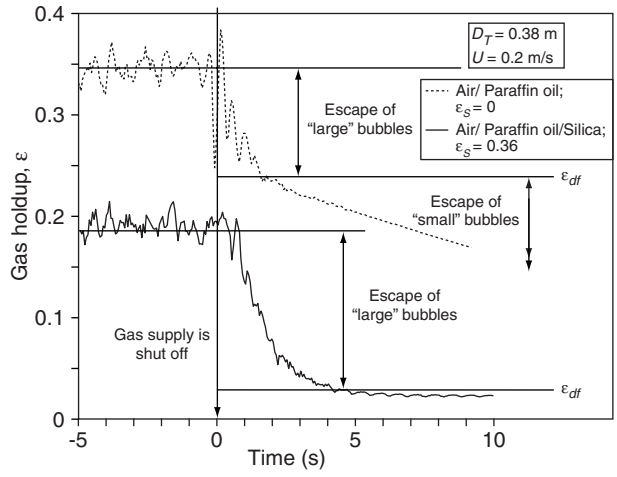

Figure 34

Dynamic gas disengagement experiments for air/paraffin oil and air/36 vol% paraffin oil slurry in a 0.38 m diameter column. The experimental data is from [20]. The system properties are as given in the legend to Figure 33.

part of the solid phase. Note the sharp maximum in the total gas holdup near the regime transition point for slurry concentrations smaller than 10%.

The dynamic gas disengagement experiment [15-20] allows us to determine the holdup of gas in the "small" and "large" bubbles. In this experiment the gas supply to a column operating under steady-state is switched off instantaneously at time $t = 0$ and the dispersion height is monitored as a function of time by means of a pressure sensor located in the column at a given height. Typical dynamic gas disengagement profiles for air-paraffin oil and air-36 vol% paraffin oil slurry in a 0.38 m column for the churn-turbulent flow regime of operation are shown in Figure 34. After the shut-off of the gas supply, the holdup decreases due to the escape of fast-rising "large" bubbles ("dilute" phase). When the "large" bubbles have escaped, the "small" bubbles leave the column. The voidage of gas in the "dense" phase, ε_{df}, is determined as indicated in Figure 34. The gas holdup of the "large" bubbles, *i.e.* "dilute" phase, is obtained from $\varepsilon_{b,\,\mathrm{large}} = (\varepsilon - \varepsilon_{df})/(1 - \varepsilon_{df})$. The terminology of "dilute" and "dense" phases is based on the "two-phase" model adopted earlier to describe the hydrodynamics of bubble columns in the churn-turbulent flow regime experiments [15-20]; this model is adapted for slurry bubble columns in Figure 35. The slope of the second, slowly disengaging portion of the bed collapse curves in Figure 34 yields the superficial gas velocity through the dense phase, U_{df}. The superficial gas velocity through the "dense" phase, U_{df}, can be taken to be equal to U_{trans}.

It is clear from the dynamic gas disengagement experiment shown in Figure 34 that the decrease in the total gas holdup in more concentrated slurries is caused primarily

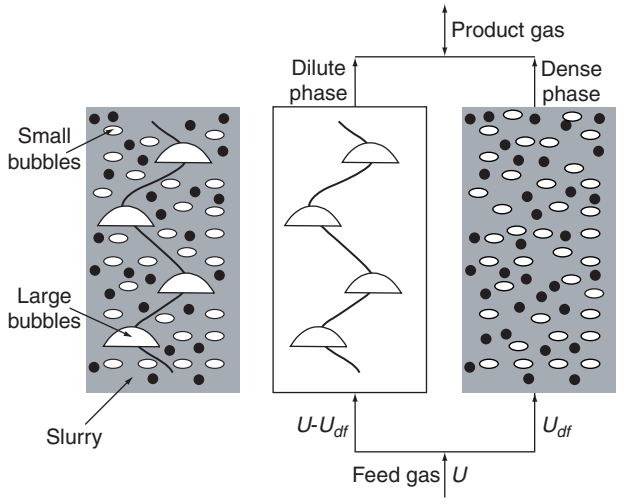

Figure 35

Generalised two-phase model applied to a bubble column slurry reactor operating in the churn-turbulent regime [20].

by the decrease in the holdup of the *small* bubbles, due to enhanced coalescence caused by the presence of the small particles. The destruction of the small bubble population is clearly demonstrated by the video imaging experiments carried out by De Swart *et al.* [18] in a two-dimensional column *(Fig. 36)*. We note that the small bubble population is virtually destroyed as the slurry concentration approaches 30 vol%. This provides an explanation of the significant decrease in the gas holdup with increasing slurry concentration as observed in Figure 33.

Data on the gas holdup in the dense phase (small bubbles) are shown in Figure 37 for the 0.38 m diameter column. Figure 37 shows that the dense phase gas holdup is approximately constant for churn-turbulent operation at superficial gas velocities exceeding about 0.1 m/s. This is a useful conclusion for scale-up purposes. Furthermore, Figure 38a shows the collection of data on the gas holdup in the dense phase, ε_{df}, for all column diameters and slurry concentrations [20]. We see that the dense phase gas holdup ε_{df} is virtually independent of the column diameter and is a significant decreasing function of the particle concentration ε_s. The unique dependence of the decrease in the dense phase gas voidage ε_{df} with increasing solids volume fraction ε_s is useful for scale-up purposes because this parameter can be determined in a relatively small diameter column under actual reaction conditions of temperature and pressure. It is clear that addition of silica particles has the effect of reducing the small bubble population virtually to zero when the slurry concentration approaches 40 vol%. The addition of solid particles tends to promote coalescence of small bubbles and the rise velocity of the small bubbles, $V_{b,\,\mathrm{small}}$, increases with increasing ε_s *(Fig. 38b)*. The paraffin-oil slurry data on the dense phase voidage ε_{df} and the small bubble rise velocity V_{small} can be correlated as:

$$\varepsilon_{df} = \varepsilon_{df,\,0}\left(1 - \frac{0.7}{\varepsilon_{df,\,0}}\,\varepsilon_s\right) \tag{25}$$

$$V_{b,\,\mathrm{small}} = V_{b,\,\mathrm{small},\,0}\left(1 + \frac{0.8}{V_{b,\,\mathrm{small},\,0}}\,\varepsilon_s\right) \tag{26}$$

where the paraffin-oil parameters $\varepsilon_{df,\,0} = 0.27$ and $V_{b,\,\mathrm{small},\,0} = 0.095$ m/s. The superficial gas velocity through the dense phase *(Fig. 35)* can be estimated from $U_{df} = V_{b,\,\mathrm{small}}\,\varepsilon_{df}$ *(Fig.38c)*.

We note from the data in Figure 39 that the *large* bubble gas holdup $\varepsilon_{b,\,\mathrm{large}}$ is practically independent of slurry concentration in the range $0.16 < \varepsilon_s < 0.36$. This is again a useful scale-up rule. From Figure 38a we note that for slurry concentrations exceeding 30 vol%, *i.e.* $\varepsilon_s > 0.30$, the small bubble population is almost completely destroyed. The total gas holdup is then made up of only large bubbles. In Figure 40 we compare the total gas holdup for $\varepsilon_s = 0.36$ with the measurements of ε in the system air-Tellus oil. We note that the total gas holdups ε in these two systems are close to one another for all three column diameters. Since the total gas holdup is determined by the rise velocity of large bubbles, Figure 40 would suggest that the large bubble rise velocity in concentrated slurries is virtually the same as in Tellus oil, and that the scale dependence is the same. This is

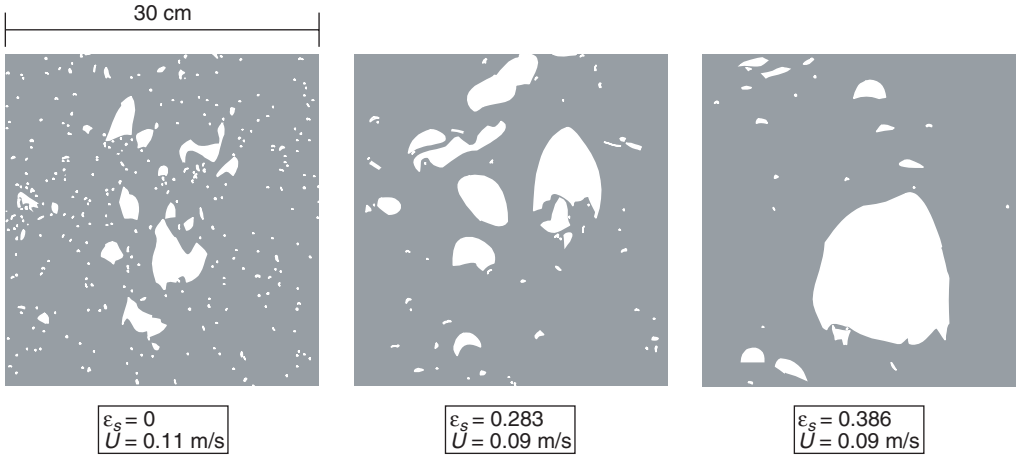

Figure 36
Influence of increased solids concentration on the gas holdup structure for air/paraffin oil slurries. Retraced video images of the hydrodynamics in a two-dimensional slurry bubble column. Experimental data from [18].

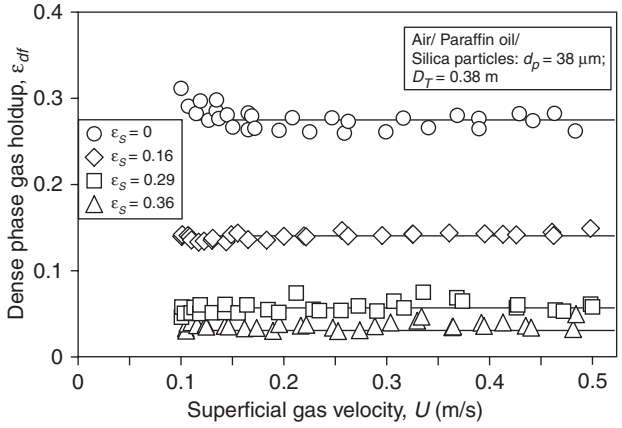

Figure 37

Influence of increased solids concentration on the dense phase gas holdup for air/paraffin oil slurries in a 0.38 m diameter column. The experimental data is from [20]. The system properties are as given in the legend to Figure 33.

confirmed by comparing the dynamic gas disengagement curves for concentrated slurries and Tellus oil at the same operating conditions *(Fig. 41)*. One must therefore conclude that the earlier determined acceleration factor *AF* for Tellus oil, given by Equation (12), would hold also for large bubble swarms in concentrated slurries. This hypothesis is confirmed by comparison of the predictions of the large bubble swarm velocity using Equations (4), (5), (9), (10) and (12) with measurements of $V_{b,\,\mathrm{large}}$ in columns of 0.1, 0.19 and 0.38 m diameter for paraffin-oil slurries with concentration $0.16 < \varepsilon_s < 0.36$ *(Fig. 42)*.

The prediction of the total gas holdup in slurry bubble columns requires estimation of the dense phase holdup ε_{df} using Equation (25). As an example, Figure 43 compares the total gas holdup estimations with experimental data in a 0.38 m diameter column with 20 vol% slurry. The agreement is good except in the region of the regime transition point.

The above model developed for the large bubble holdup is adequate for scale up slurry bubble columns operating at ambient pressure conditions. For high-pressure operation, the model needs to be modified to take account of the influence of increased system pressure on ε_{df}, U_{df} and on $V_{b,\,\mathrm{large}}$.

From Equations (18) and (19) we note that increased pressure (or gas density) tends to increase ε_{df} whereas from Equation (25) increased catalyst concentration ε_s tends to reduce ε_{df}. These two effects can be combined into a formula:

$$\varepsilon_{df} = \varepsilon_{df,\,0}\left(\frac{\rho_G}{\rho_{G,\,\mathrm{ref}}}\right)^{0.48}\left(1-\frac{0.7}{\varepsilon_{df,\,0}}\varepsilon_s\right) \qquad (27)$$

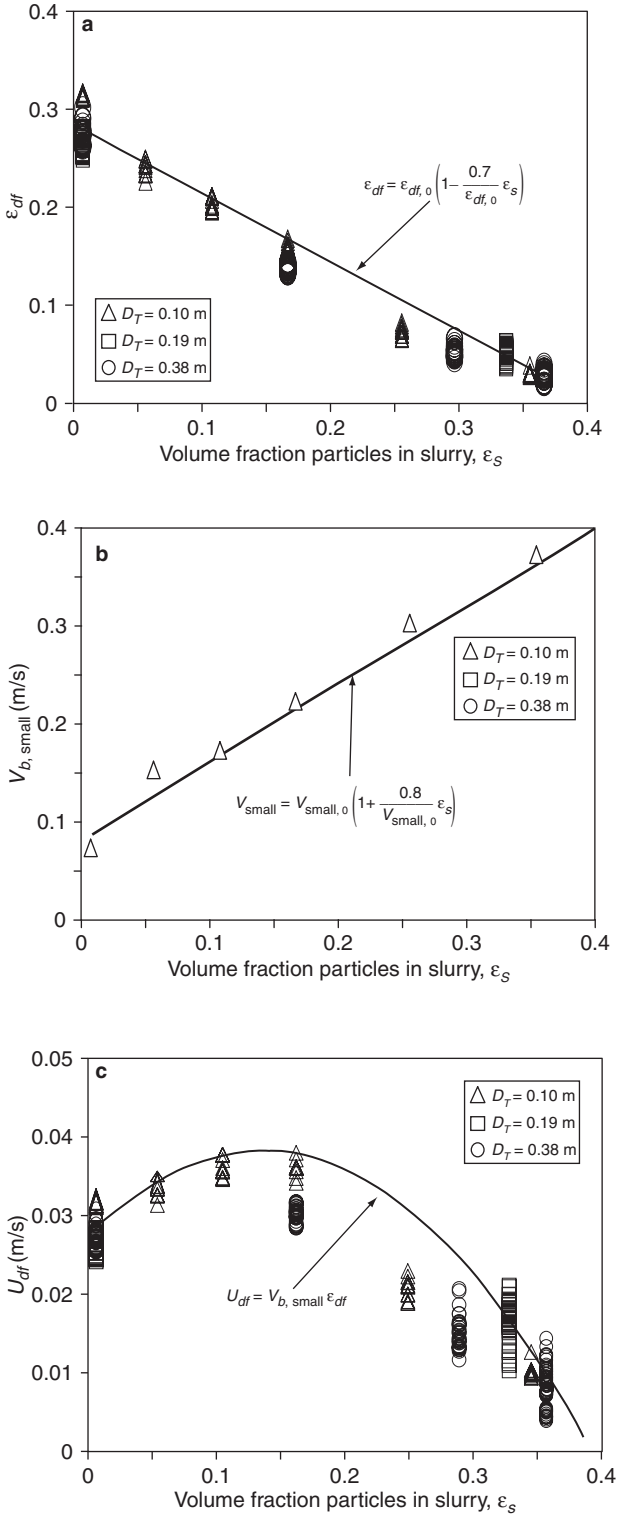

Figure 38

Influence of particles concentration ε_s on (a) dense phase gas voidage, ε_{df}, (b) rise velocity of the small bubbles, V_{small} and (c) superficial gas velocity through the dense phase U_{df}. The experimental data is from [20]. The system properties are as given in the legend to Figure 33.

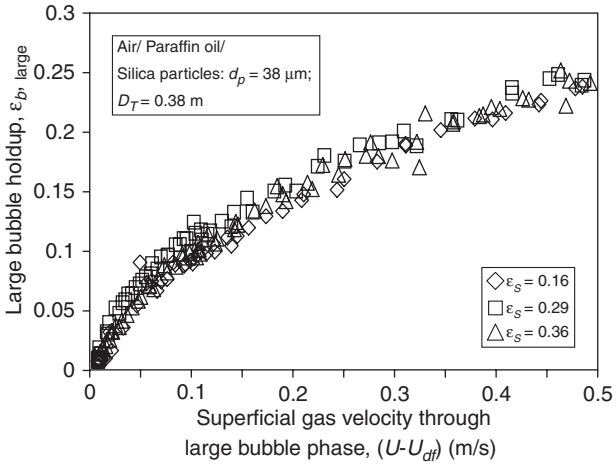

Figure 39

Large bubble gas holdup in a 0.38 m diameter column for various slurry concentrations. The experimental data is from [20]. The system properties are as given in the legend to Figure 33.

where $\rho_{G,\ ref}$ is the density of gas at ambient conditions (= 1.29 kg/m^3 in usual experimental work with air at atmospheric pressure as the gas phase). In pure liquids the "small" bubble rise velocity $V_{b,\ small,\ 0}$ is only very weakly dependent on the gas density. The superficial gas velocity through the dense phase, $U_{df} = V_{b,\ small}\ \varepsilon_{df}$, for slurry systems at elevated pressures can be calculated by combining Equations (26) and (27).

The influence of increased pressure (gas density) on the large bubble holdup in slurry bubble columns can be accounted for by the density correction factor and use of Equations (23) and (24).

2 MASS TRANSFER FROM THE BUBBLES TO THE LIQUID

Due to the small size of catalyst particles in slurry reactors (particle diameter typically of the order of 50 μm), intraparticle diffusion is not a limiting factor. With catalysts of relatively low activity present in low concentration in bubble columns operated in the homogeneous regime, gas-liquid mass transfer is unlikely to be a limiting factor either in view of the large surface area of the small bubbles or their long residence time in the liquid. However, for reactors of increased productivity, because of the use of more active catalysts in high concentrations and operation in the heterogeneous regime, gas-liquid mass transfer becomes a factor that needs serious consideration. Conventional calculation of mass transfer rates based on the application of the surface renewal theory with the holdup and size of the

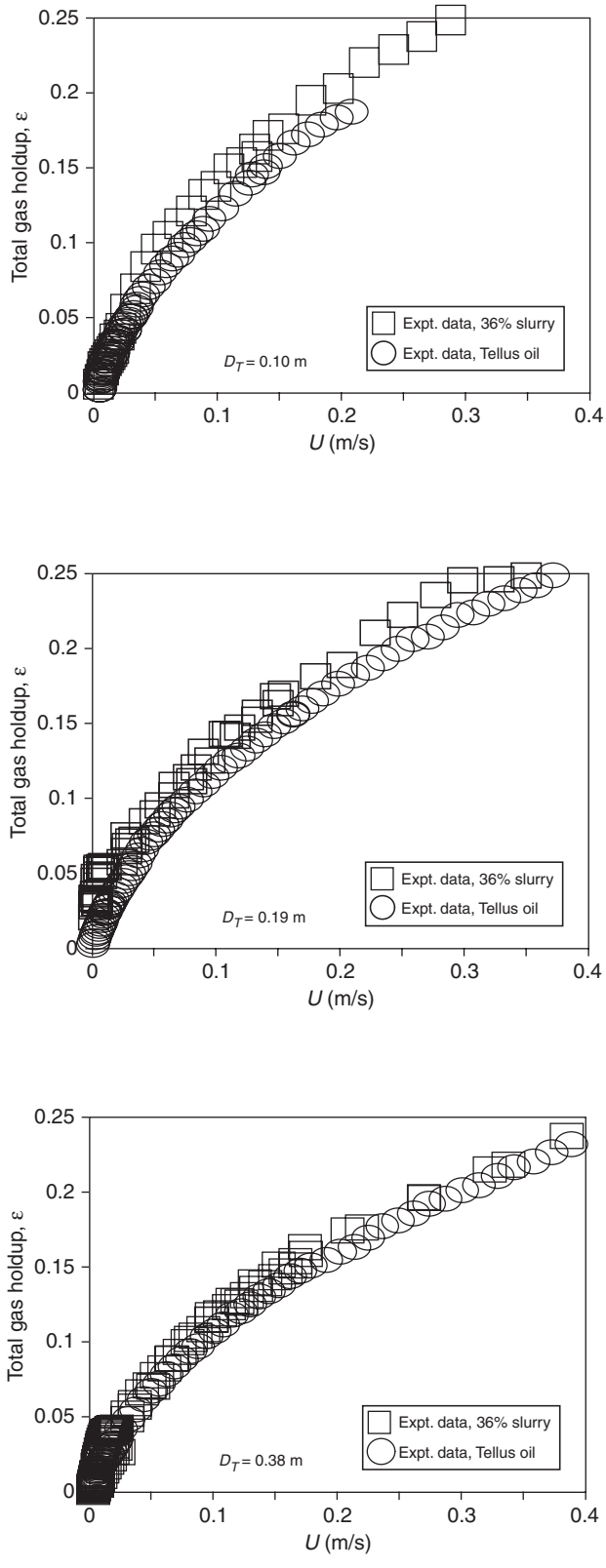

Figure 40

Comparison of the total gas holdup for 36 vol% paraffin slurry with measurements using air-Tellus oil.

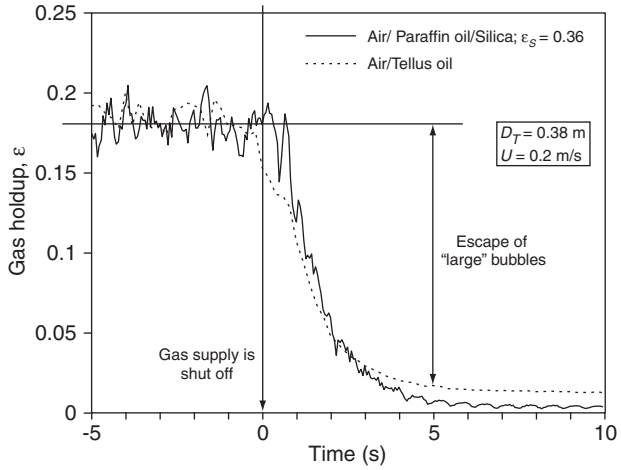

Figure 41

Comparison of dynamic gas disengagement curves for 36 vol% paraffin slurry with measurements using air-Tellus oil.

large bubbles (which represent the major part of the gas throughput) as input yields relatively low rates which would considerably detract from the attractiveness of bubble columns as Fischer-Tropsch reactors. Experimental data obtained on model systems would seem to suggest that the situation is not as bleak, however, since actual rates are found to be higher than calculated ones by a factor of 5 to 10. Experimental gas-liquid mass transfer rates for turpentine-nitrogen in the heterogeneous regime were found to be an order of magnitude higher than estimated on the basis of correlations that have been established for small bubbles mainly [9].

Letzel *et al.* [31] measured the volumetric mass transfer coefficient k_La for the air-water system at various system pressures. Their experimental data *(Fig. 44)* showed that the whole data set could be approximated by the simple relation:

$$\frac{k_La}{\varepsilon} \approx 0.5 \qquad (28)$$

for both homogeneous and heterogeneous regimes of operation. The relation (28), which stems from the early work of Vermeer and Krishna [9], implies that there is no detrimental effect accruing from operation in the heterogeneous flow regime. This appears to be paradoxical at first sight because for heterogeneous regime of operation one observes bubbles in the range 20-50 mm in size, an order of magnitude larger than in the homogeneous flow regime.

An explanation for this paradox was obtained in the work of De Swart *et al.* [18], using high-speed video imaging techniques to study the dynamics of large bubbles in concentrated slurries. In these studies it was observed that within the class of large bubbles, bubbles of a given size do

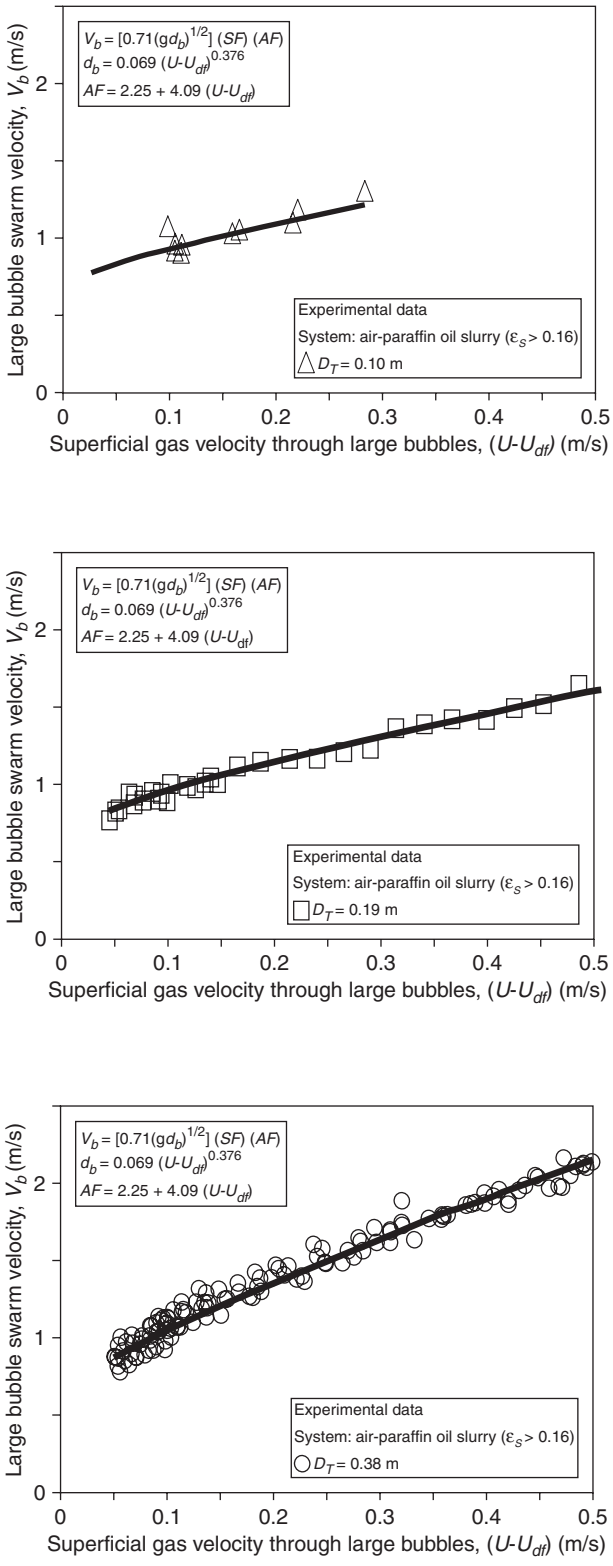

Figure 42

Influence of column diameter on the rise velocity of large bubbles V_b in paraffin oil slurries. Experimental data compared with predictions of model using Equations (4), (5), (9), (10) and (12).

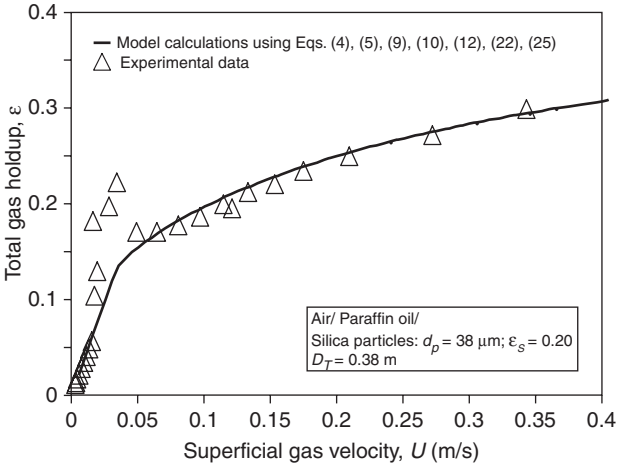

Figure 43

Estimation of the total gas holdup for a 20 vol% slurry in a 0.38 m diameter column compared with experimental data. Estimations using Equations (4), (5), (9), (10), (12), (22) and (25).

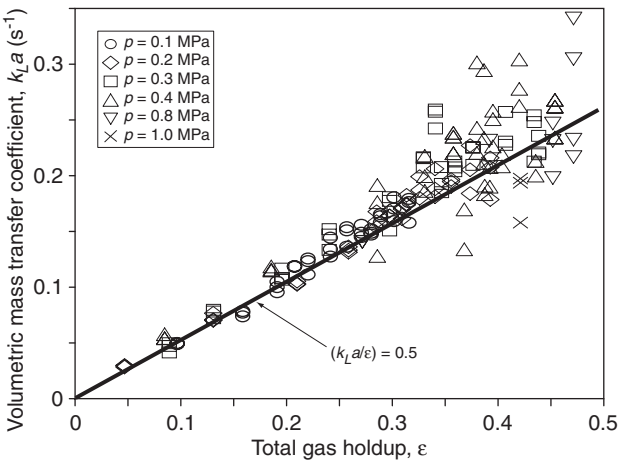

Figure 44

Data on volumetric mass transfer coefficient k_La at various system pressures for the air-water system in a 0.15 m diameter column [31].

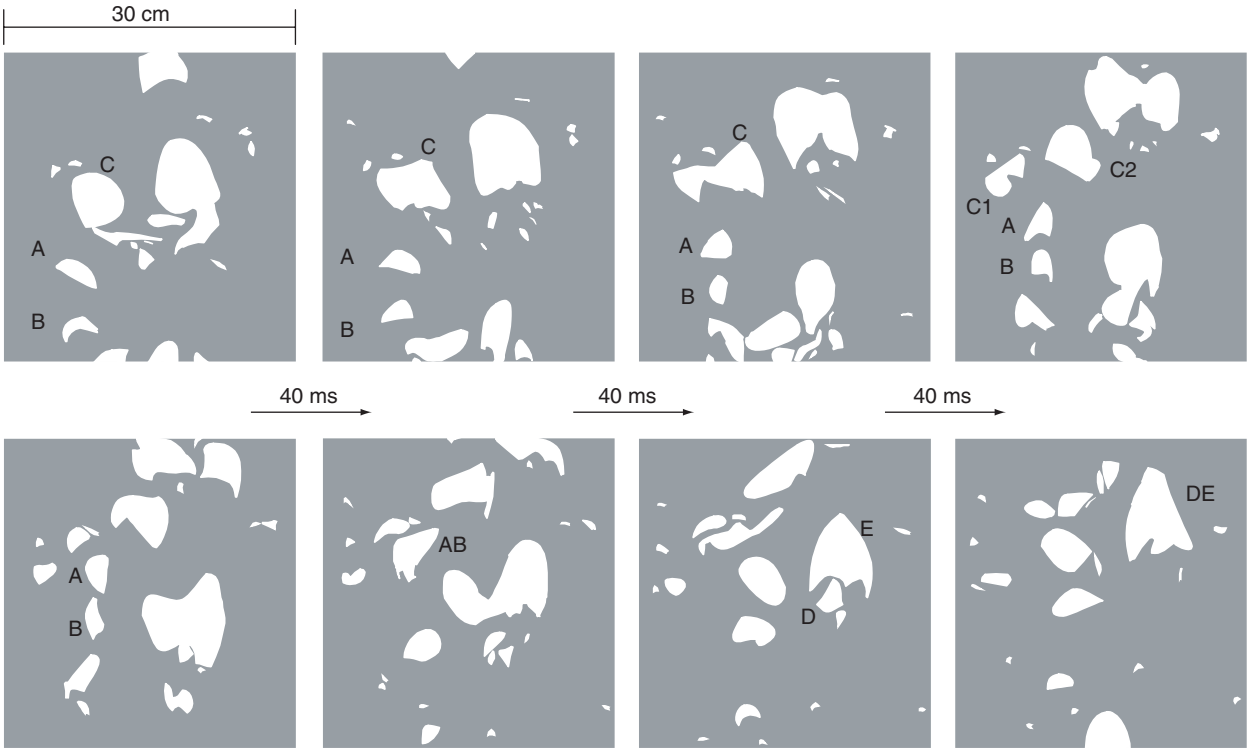

Figure 45

Bubble coalescence and bubble breakup as followed by video recording, at 25 frames per second, in a two-dimensional slurry bubble column. Eight consecutive frames of the air/28.3 vol% paraffin oil slurry. Recorded at a height of 0.65 m and a superficial gas velocity of 0.09 m/s [18].

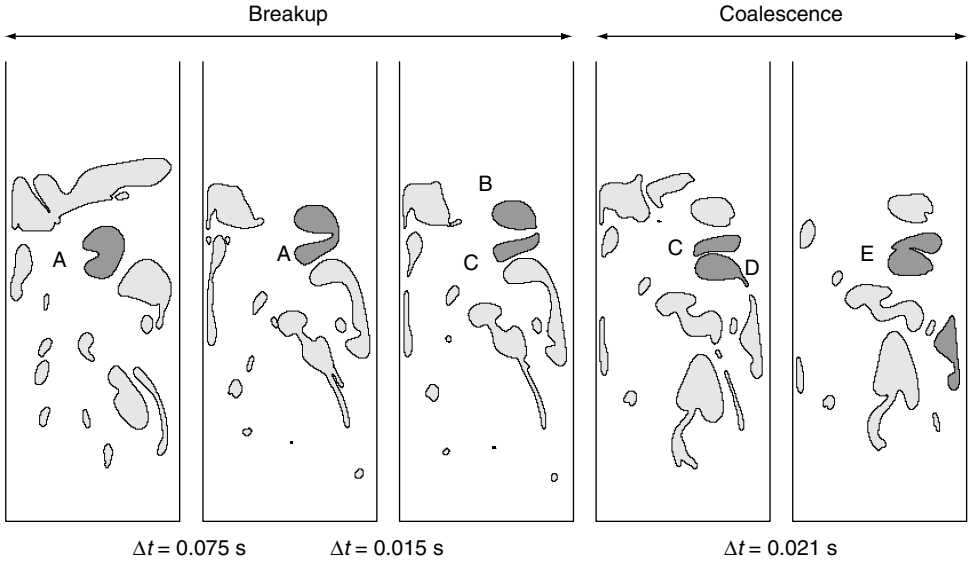

Figure 46

VOF simulations of coalescence and breakup in a 2D column of 0.3 m width. The animations of these simulations, along with details of the simulations, are to be found on our web site (http://ct-cr4.chem.uva.nl/breakup/). Details of these simulations are to be found in [37].

not lead an isolated life, but are continually disappearing and reappearing as a result of breakup and coalescence. Figure 45 shows eight sequential pictures (frames) taken from an experimental run in a two-dimensional column of 0.3 m width operating with a 28.3 vol% paraffin oil slurry at a superficial gas velocity of 0.09 m/s. The time interval between the individual frames is 40 ms and the "small" bubbles, smaller than 10 mm, have been filtered out. Two bubbles A and B are followed as they rise through the column. It can be seen from frames 1 to 4 that bubble B rises faster than bubble A. In frame 5 bubble B reaches the wake of bubble A and coalescence follows; in frame 6, A and B are coalesced and bubble AB is formed. Bubbles D and E in frame 7 coalesce to form DE in frame 8. Tracking the history of bubble C in frames 1, 2, 3 and 4, it is noted that in frame 4 bubble C breaks up into bubbles C1 and C2. VOF simulations of bubble coalescence and breakup in an air-water system *(Fig.46)* confirm the frequent coalescence and breakup of "large" bubbles. De Swart *et al.* [18] also determined that the exchange of gas between various bubble classes occurs at a very high rate, at least 4 s^{-1}, which is higher than the characteristic renewal rate for mass transfer. Put another way, during the characteristic time for mass transfer from the gas to the liquid phase, a bubble loses its identity because of frequent exchanges with gas in other bubble size classes. Thus, whereas the gas throughput is mainly represented by the largest bubbles, gas-liquid mass transfer is largely determined by the interfacial area of the smaller bubbles. In other words, the equivalent bubble size as regards mass transfer is relatively small and small enough for mass transfer not to be a limiting factor in Fischer-Tropsch synthesis in most cases.

The influence of bubble-bubble exchanges is illustrated by simulations carried out for conditions relevant for the Fischer-Tropsch synthesis [18]. Hydrogen absorption from synthesis gas into paraffin oil at a pressure of 40 bar and a temperature of 513 K is considered. Hydrogen and carbon monoxide are present in the syngas feed at a ratio of 2. The superficial gas velocity through the total large bubble population, of 0.079 m/s, is assumed to be constant over the reactor height of 30 m. Figure 47 shows the dimensionless hydrogen concentration $C_{g.H2}/C_{g0.H2}$ profile along the column height obtained for each of three bubble size classes: 0.01, 0.04 and 0.1 m in diameter. The three profiles coincide with one another because of very frequent exchange rates between the bubble classes and the conversion at the reactor outlet is 68%. The conversion behaviour of the three-bubble class system, with 0.01, 0.04 and 0.1 m diameter bubbles is found equivalent to that of a single bubble class system of diameter 0.021 m. Put another way, due to frequent bubble-bubble interchanges the effective bubble diameters for the 0.04 and 0.1 m diameter classes are reduced to about 0.02. This implies an enhancement for the 0.1 m bubble class of a factor equal to 5. In order to further demonstrate the significance of the bubble-bubble interchange, simulations were also carried out assuming no exchanges between the three bubble classes. The results of this model are shown as dashed line in Figure 47. The overall conversion achieved

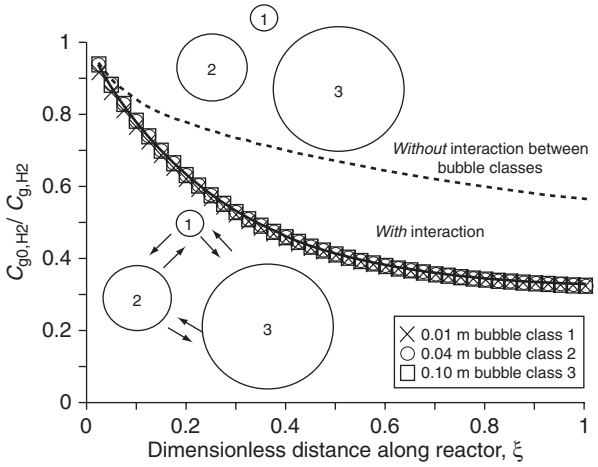

Figure 47

Effect of bubble-bubble interaction on axial concentration profiles of hydrogen concentration in the bubbles as determined by computer modelling [18]. The dashed line represents the profile obtained when the interaction between the three assumed bubble classes is negligible.

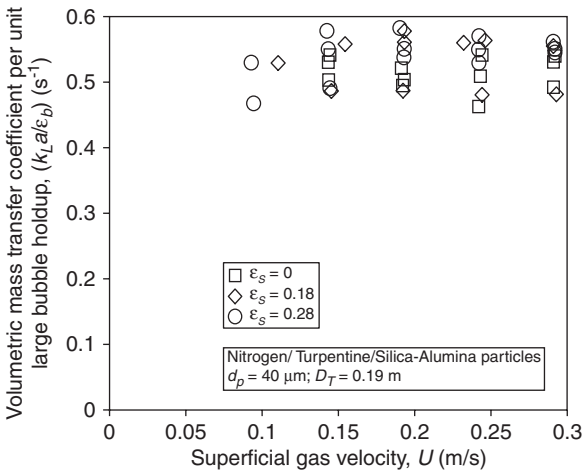

Figure 48

Mass transfer data in slurry bubble columns. Unpublished data of Krishna.

by the non-exchanging bubble ensemble is only 43%, significantly lower than that obtained taking interactions into account.

For a bubble column reactor operating with concentrated slurry in the heterogeneous flow regime at elevated pressures, the relation (28) can be applied after applying two corrections. Firstly, the total gas holdup is predominantly made up of large bubbles and so $\varepsilon \approx \varepsilon_b$. Secondly, the mass transfer coefficient needs to be corrected for the liquid phase diffusivity under the actual conditions prevailing in the Fischer-Tropsch reactor:

$$\frac{k_L a}{\varepsilon_b} = 0.5\sqrt{\frac{Đ_L}{Đ_{L,\,\mathrm{ref}}}} \tag{29}$$

where $Đ_L$ is the diffusion coefficient in the liquid phase, while $Đ_{L,\,\mathrm{ref}}$ is equal to 2×10^{-9} m^2/s (valid for the measurement systems in Vermeer and Krishna [9]). The diffusivities $Đ_L$ of the H_2 and CO species at a reaction temperature of say 240°C are 45.5×10^{-9} and 17.2×10^{-9} m^2/s respectively. The validity of Equation (29) for slurry bubble columns is demonstrated by the experimental data presented in Figure 48.

3 BACKMIXING OF THE LIQUID PHASE

For churn-turbulent regime operation, the large bubbles tend to concentrate near the centre of the column and carry liquid (slurry) upwards in their wake. At the top of the dispersion, the large bubbles disengage and the liquid (slurry) is recirculated. Figure 49 shows the measured radial liquid velocity distribution $V_L(r)$ for the three columns operating at a superficial gas velocity of 0.23 m/s with the air-water system. The strong influence of the column diameter is evident. We note the strong downwardly directed liquid velocity in the wall region and the upwardly directed velocity in the central core. This liquid re-circulation is the cause of liquid phase dispersion and backmixing. If all the measured $V_L(r)$ data for air-water systems are normalised with respect to the centre-line velocity $V_L(0)$, we see that the radial distributions are all similar *(Fig. 50)*. The important conclusion to be drawn from the result in Figure 50 is that the magnitude of re-circulatory flows can be characterised by a single velocity, say the centre-line liquid $V_L(0)$. This would suggest that the liquid phase dispersion coefficient $D_{ax,L}$ should be proportional to $V_L(0)$. Figure 51a compares the estimations of $V_L(0)$ using various literature correlations [54-62] with experimental data. Of the literature correlations we consider the one due to Riquarts [59]:

$$V_L(0) = 0.21(\mathrm{g}D_T)^{\frac{1}{2}}\left(\frac{U^3}{\mathrm{g}\nu_L}\right)^{\frac{1}{8}} \tag{30}$$

as most suitable for estimation purposes. According to Equation (30) the centre-line velocity $V_L(0)$ should increase monotonously with the square root of column diameter D_T *(Fig. 51b)*. The accuracy of this extrapolation is crucial to

successful scale-up. In order to test this extrapolation, CFD simulations were carried out in the Eulerian framework defining three phases (small bubbles, large bubbles and liquid) as shown in Figure 24. The drag between the small bubbles and liquid were determined from:

$$C_{D,\,\mathrm{small}} = \frac{4}{3}\,\frac{\rho_L - \rho_G}{\rho_L}\,g d_{b,\,\mathrm{small}}\,\frac{1}{V^2_{b,\,\mathrm{small}}} \tag{31}$$

where $V_{b,\,\mathrm{small}}$ was estimated using the Harmathy relation (15), and taking the small bubble diameter to be 4 mm. For the large bubbles the drag coefficient is estimated from:

$$C_{D,\,\mathrm{large}} = \frac{4}{3}\,\frac{\rho_L - \rho_G}{\rho_L}\,g d_{b,\,\mathrm{large}}\,\frac{1}{V^2_{b,\,\mathrm{large}}} \tag{32}$$

using Equations (4), (5), (9)-(11) for the estimation of the large bubble velocity. The only other unknown parameter in

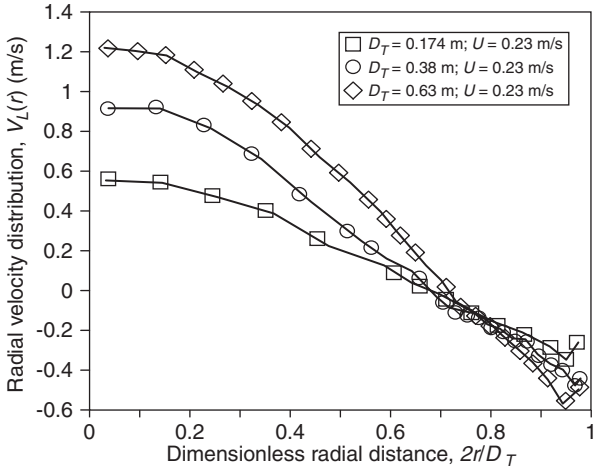

Figure 49

Radial distribution of the axial component of the liquid velocity at a superficial gas velocity U = 0.23 m/s for three column diameters with the air-water system. Measurements using a modified Pitot tube [33].

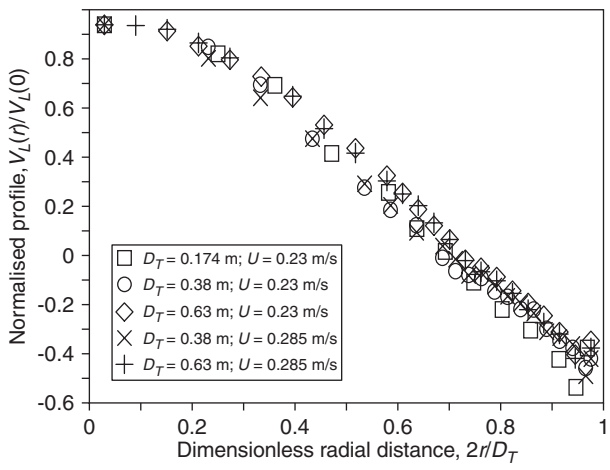

Figure 50

Normalised radial velocity distribution profiles for air-water system. Measurements using a modified Pitot tube [33].

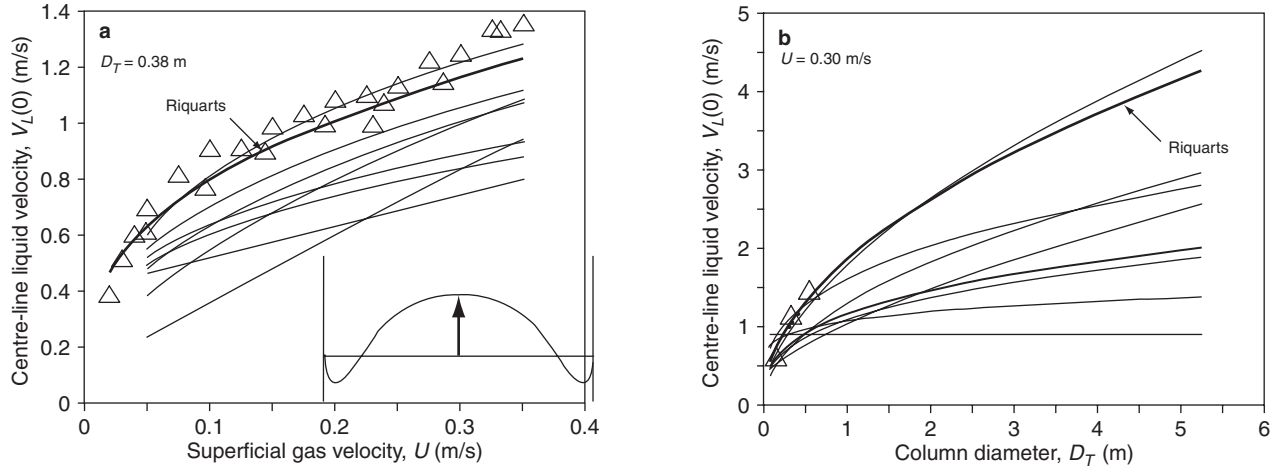

Figure 51

Comparison of literature correlations for the centre-line velocity $V_L(0)$ for air-water system with experimental data.
(a) Variation of $V_L(0)$ with superficial gas velocity for a column of 0.38 m diameter.
(b) Variation of $V_L(0)$ with column diameter for a superficial gas velocity of 0.30 m/s.
The plotted correlations are to be found in [54-62].

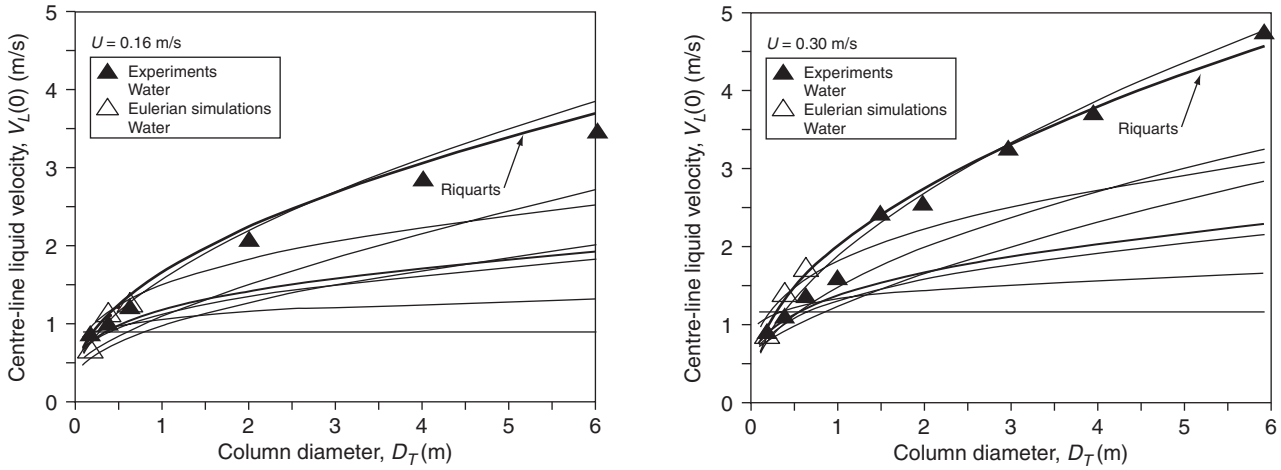

Figure 52

Variation of $V_L(0)$ with column diameter for superficial gas velocities of 0.16 and 0.30 m/s. Comparison of literature correlations for the centre-line velocity $V_L(0)$ for air-water system with Eulerian simulations. The plotted correlations are the same as in the legend to Figure 51.

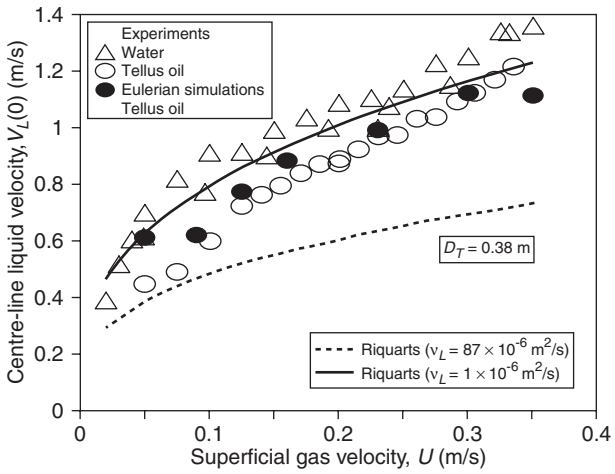

Figure 53

Comparison of centre-line velocity data $V_L(0)$ for air-water and air-Tellus oil systems in a 0.38 m diameter with Riquarts correlation [59] and Eulerian simulations with Tellus oil. Details of these simulations are to be found in [38].

the model represented in Figure 24 is the transition gas velocity, U_{trans}. This value was taken to be 0.034 m/s in the simulations shown in Figure 52 for various column diameters operating at U = 0.16 m/s and 0.3 m/s. The Eulerian simulations seem to confirm the validity of the Riquarts correlation for a range of column diameters up to 6 m.

Riquarts correlation (30) anticipates a dependence of $V_L(0)$ on the kinematic viscosity of the liquid phase, ν_L. However, the experimental data of Krishna *et al.* [33, 38] shows that the liquid viscosity does not have any significant influence on the centre-line velocity $V_L(0)$ *(Fig. 53)*. We therefore recommend the use of Equation (30) for all systems taking $\nu_L = 10^{-6}$ m^2/s.

Since we had earlier shown the hydrodynamics of Tellus oil to be similar to that of highly concentrated slurries (36 vol% concentration), the inescapable conclusion to be drawn is that $V_L(0)$ for concentrated slurry bubble columns can be estimated using Equation (30), but taking $\nu_L = 10^{-6}$ m^2/s. Three-phase Eulerian simulations (taking $U_{trans} \approx 0$) confirm that Equation (30) with water properties is capable of predicting the scale dependence of $V_L(0)$ *(Fig. 54)*. A remarkable result observed from Figure 54b is that a Fischer-Tropsch slurry reactor of 6 m diameter operating at a superficial gas velocity of 0.3 m/s has a centre-line velocity $V_L(0)$ of 4.4 m/s!

Figure 55 compares the radial liquid velocity distribution in a column of 0.38 m diameter for air-water and air-Tellus oil. Interestingly, the profiles are indistinguishable from each other, confirming the idea that liquid viscosity does not influence either $V_L(0)$ or $V_L(r)$. These profiles will also hold for concentrated slurries.

Another remarkable conclusion to be drawn is that the slurry phase backmixing is the same as for low viscosity liquids such as water. Measured experimental data [33, 63-66] for the liquid phase axial dispersion coefficient $D_{ax,\,L}$ show that this parameter is a simple product of the centre-line liquid velocity $V_L(0)$ and column diameter D_T:

$$D_{ax,\,L} = 0.31\, V_L(0)\, D_T \qquad (33)$$

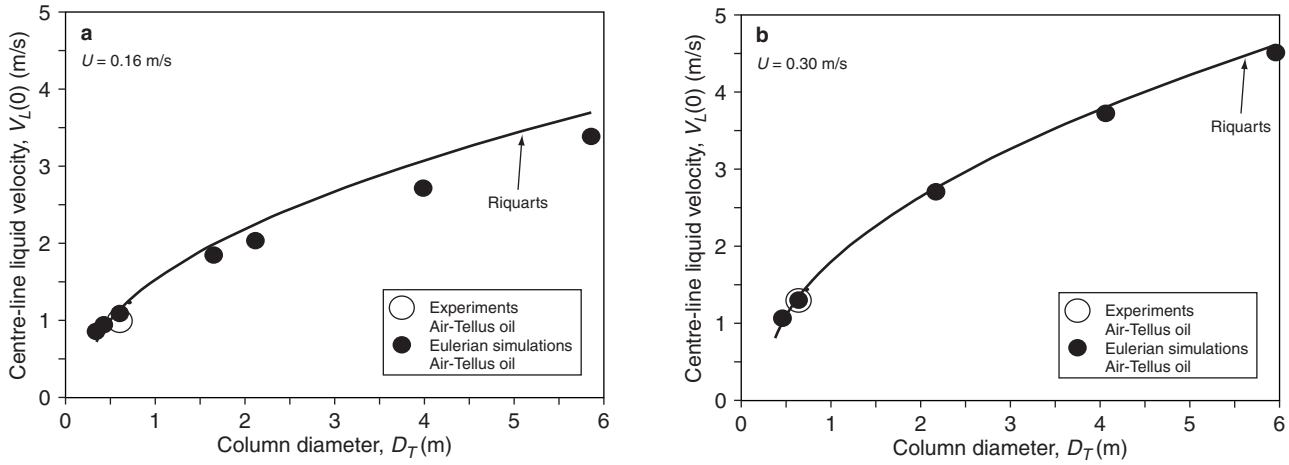

Figure 54

Variation of $V_L(0)$ with column diameter for superficial gas velocities of (a) 0.16 m/s and (b) 0.30 m/s. Comparison of Riquarts correlation [59] for the centre-line velocity $V_L(0)$ for air-Tellus oil system with Eulerian simulations. Details of these simulations are to be found in [38].

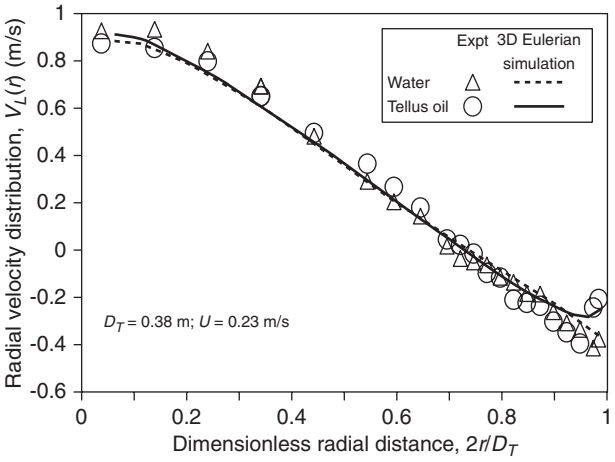

Figure 55

Radial distribution of the axial component of the liquid velocity at a superficial gas velocity U = 0.23 m/s for air-water and air-Tellus oil systems measured in a 0.38 m diameter column. Measurements using a modified Pitot tube [33, 38]. Also shown with continuous lines are the results of fully three-dimensional Eulerian simulations [36]. Details of the simulations, including animations, are available on our web site (http://ct-cr4.chem.uva.nl/oil-water).

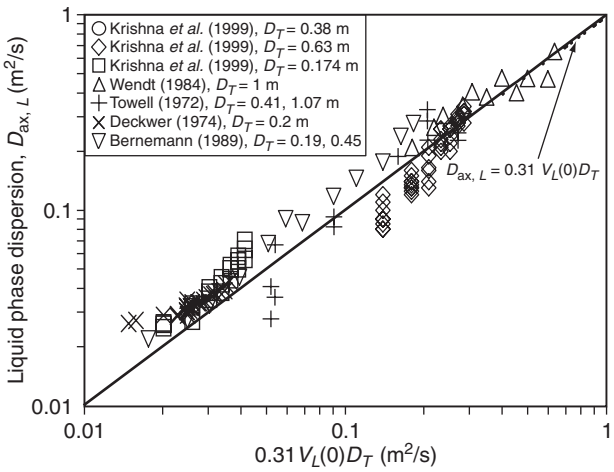

Figure 56

Axial dispersion coefficient of the liquid phase. Comparison of experimental data [39, 41, 50-53] with the correlation $D_{ax,\,L} = 0.31\ V_L(0)\ D_T$, wherein the centre-line liquid velocity is estimated from the Riquarts correlation (15) taking $\mu_L = 10^{-6}$ m²/s.

where we take Equation (30), using the kinematic viscosity of water at room temperature, for estimation of $V_L(0)$.

The comparison of Equation (33) with literature data is shown in Figure 56.

For a commercial scale bubble column slurry reactor of diameter D_T = 7 m operating at U = 0.35 m/s, Equations (15) and (16) yield an estimate $D_{ax,\,L}$ = 10 m²/s, suggesting that the "dense" phase can be considered to be well mixed.

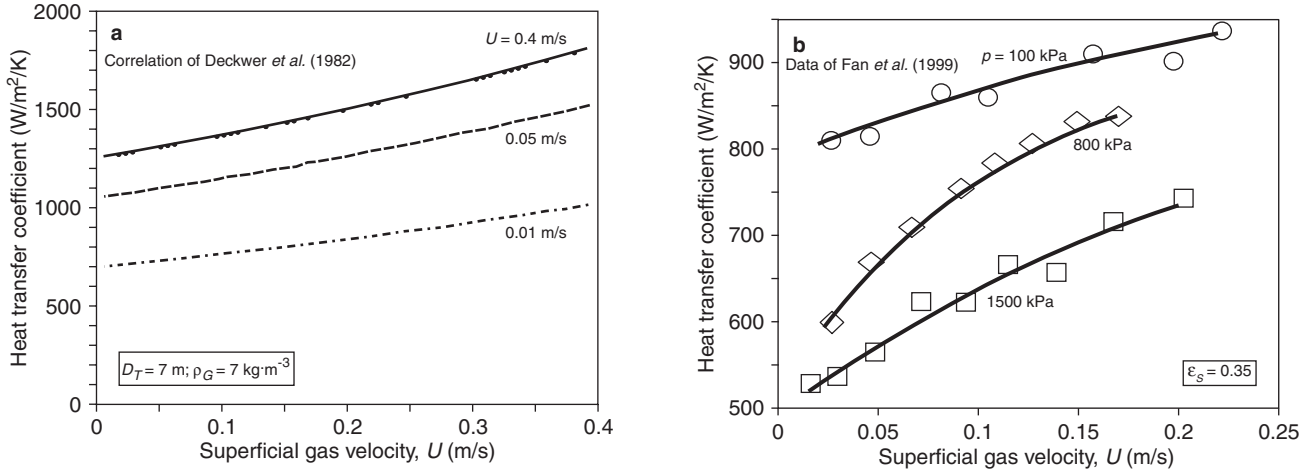

Figure 57

Heat transfer coefficients to cooling tubes in slurry reactors.
(a) Correlation from [67].
(b) Data from [68].

4 HEAT TRANSFER IN BUBBLE COLUMNS

The effective heat transfer and the good temperature equalisation in a slurry bubble column, particularly when operated in the heterogeneous regime, are important advantages of this type of reactor. Heat transfer coefficients in the region of 1000 W/m^2/K can be obtained as can be seen from the estimations in Figure 57a which are based on the Deckwer *et al.* [67] correlation, adapted to take more recent insights into slurry column hydrodynamics. It can be seen that the heat transfer coefficient increases with increasing gas velocity and with increasing solids concentration, *i.e.*, with factors which favour the heterogeneous regime. More recent work by Fan *et al.* [68] has shown that the heat transfer coefficient is also affected by the system pressure *(Fig. 57b)*. However, no correlation for heat transfer coefficient has been developed.

5 OPERATIONAL ASPECTS OF SLURRY BUBBLE COLUMNS

There are several operational aspects of bubble column slurry reactors that deserve attention:

– catalyst loading and unloading in bubble column slurry reactors is much easier than in multi-tubular fixed bed reactors and can be accomplished in a shorter time. Moreover, the activity of the catalyst inventory in the reactor can be maintained by withdrawal of catalyst and replacement with fresh catalyst during a run;
– in the case of the synthesis of heavy Fischer-Tropsch products, separation of solids from the liquid in the slurry reactor technology may not be a trivial problem. Distilling off the product is not possible with heavy liquids, and filtering may prove necessary. The separation problem is aggravated if fines are produced by catalyst attrition (either mechanical or chemical attrition);
– foam formation is obviously a problem to be avoided in a bubble column Fischer-Tropsch reactor;
– at too low velocities, a concentration gradient of catalyst may develop in a slurry reactor and this may limit the turndown ratio. Deposition of insoluble, sticky material onto the catalyst particles may hamper proper suspension of the catalyst.

CONCLUDING REMARKS

The Fischer-Tropsch bubble column slurry reactor is the most attractive option for large scale commercial application. The slurry bubble column is best operated in the heterogeneous or churn-turbulent regime at a superficial gas velocity in the region of 0.3 m/s with highly concentrated slurries, approaching 35-40 vol% of catalyst in the slurry phase. The scale-up of the bubble column slurry reactor must be carried out with caution. The following important aspects of bubble column hydrodynamics have been emphasised in this review:

– in the heterogeneous flow regime, the dispersion consists of a variety of bubble sizes, which can be simplified into

two classes: "small" and "large". The gas throughput and conversion are mainly contributed by the large bubble population;
- the large bubble rise velocity prediction is a key factor in the scale-up; this velocity depends on scale;
- bubble interactions tend to increase the large bubble rise velocity because of wake interaction effects;
- increased system pressures delay transition to the heterogeneous flow regime and enhance the breakup of large bubbles. A density correction factor is used to describe the influence of increased gas density on the large bubble rise velocity.

Whereas the upscaling of the multi-tubular reactor from a pilot plant scale to an industrial scale is relatively straightforward and safe, this is not the case for the bubble column reactor and a costly demonstration stage is generally considered to be necessary. However, recent insights in the hydrodynamics of this reactor suggest that a rational upscaling strategy based on investigations in small "hot" pilot plants and larger "cold flow" engineering test rigs may be adopted as an alternative to the traditional, largely empirical development route. Based on the presently available knowledge, it can be expected that a bubble column Fischer-Tropsch reactor may achieve a productivity of 2500 t/d (about 20 000 bbl/d), which is a thousand times higher than that of the classical Fischer-Tropsch reactor operated in the forties.

Besides developments in reactor technology, significant improvements have also been realised in the catalysis of the Fischer-Tropsch process in recent years. A discussion of the advances in catalysis, which is rendered difficult because most information is in the domain of proprietary company know-how, is outside the scope of the present paper. However, it will be clear that the combination of advances in catalysis and reactor technology, together with innovations in syngas production, have considerably improved the prospects of large scale economic production of synthetic hydrocarbons from remote natural gas.

REFERENCES

1 Jager, B. and Espinoza, R. (1995) Advances in Low Temperature Fischer-Tropsch Synthesis. *Catalysis Today*, 23, 17-28.

2 Jager, B. (1998) Developments in Fischer-Tropsch Technology. *Studies in Surface Science and Catalysis*, **119**, 25-34.

3 Eisenberg, B., Fiato, R.A., Mauldin, C.H., Say, G.R. and Soled, S.L. (1998) Exxon's Advanced Gas-to-Liquids Technology. *Studies in Surface Science and Catalysis*, **119**, 943-948.

4 Krishna, R. and Sie, S.T. (1994) Strategies for Multiphase Reactor Selection. *Chem. Eng. Sci.*, **49**, 4029-4065.

5 Sie, S.T. (1998) Process Development and Scale up: IV. Case History of the Development of a Fischer-Tropsch Synthesis. *Reviews in Chemical Engineering*, 14, 109-157.

6 De Swart, J.W.A., Krishna, R. and Sie, S.T. (1997) Selection, Design and Scale up of the Fischer-Tropsch Slurry Reactor. *Studies in Surface Science and Catalysis*, 107, 213-218.

7 Deckwer, W.D. (1992) *Bubble Column Reactors*, John Wiley & Sons, New York.

8 Fan, L.S. (1989) *Gas-Liquid-Solid Fluidization Engineering*, Butterworths, Boston.

9 Vermeer, D.J. and Krishna, R. (1981) Hydrodynamics and Mass Transfer in Bubble Columns Operating in the Churn-Turbulent Regime. *Ind. Eng. Chem. Process Design & Dev.*, **20**, 475-482.

10 Krishna, R., Wilkinson, P.M. and Van Dierendonck, L.L. (1991) A Model for Gas Holdup in Bubble Columns Incorporating the Influence of Gas Density on Flow Regime Transitions. *Chem. Eng. Sci.*, **46**, 2491-2496.

11 Hoefsloot, H.C.J. and Krishna, R. (1993) Influence of Gas Density of Flow Regime Transitions in Homogenous Flow in Bubble Columns. *Ind. Eng. Chem. Research*, 32, 747-750.

12 Krishna, R., Ellenberger, J. and Hennephof, D.E. (1993) Analogous Description of Gas-Solid Fluidized Beds and Bubble Columns. *Chem. Eng. J.*, 53, 89-101.

13 Krishna, R., De Swart, J.W.A., Hennephof, D.E., Ellenberger, J. and Hoefsloot, H.C.J. (1994) Influence of Increased Gas Density on the Hydrodynamics of Bubble Column Reactors. *AIChE J.*, **40**, 112-119.

14 Ellenberger, J. and Krishna, R. (1994) A Unified Approach to the Scale up of Gas-Solid Fluidized and Gas-Liquid Bubble Column Reactors. *Chem. Eng. Sci.*, **49**, 5391-5411.

15 Krishna, R. and Ellenberger, J. (1995) A Unifed Approach to the Scale up of "Fluidized" Multiphase Reactors. *Chem. Eng. Research & Design, Trans. I. Chem. E.*, 73, 217-221.

16 De Swart, J.W.A. and Krishna, R. (1995) Effect of Particles Concentration on the Hydrodynamics of Bubble Column Slurry Reactors. *Chem. Eng. Research & Design, Trans. I. Chem. E.*, 73, 308-313.

17 Krishna, R., Ellenberger, J. and Sie, S.T. (1996) Reactor Development for Conversion of Natural Gas to Liquid Fuels: A Scale up Strategy Relying on Hydrodynamic Analogies. *Chem. Eng. Sci.*, **51**, 2041-2050.

18 De Swart, J.W.A., van Vliet, R.E. and Krishna, R. (1996) Size, Structure and Dynamics of "Large" Bubbles in a 2-D Slurry Bubble Column. *Chem. Eng. Sci.*, **51**, 4619-4629.

19 Krishna, R. and Ellenberger, J. (1996) Gas Holdup in Bubble Column Reactors Operating in the Churn-Turbulent Flow Regime. *AIChE J.*, **42**, 2627-2634.

20 Krishna, R., de Swart, J.W.A., Ellenberger, J., Martina, G.B. and Maretto, C. (1997) Gas Holdup in Slurry Bubble Columns. *AIChE J.*, **43**, 311-316.

21 Letzel, H.M., Schouten, J.C., van den Bleek, C.M. and Krishna, R. (1997) Influence of Elevated Pressure on the Stability of Bubbly Flows. *Chem. Eng. Sci.*, **52**, 3733-3739.

22 Letzel, H.M., Schouten, J.C., Krishna, R. and van den Bleek, C.M. (1997) Characterization of Regimes and Regime Transitions in Bubble Columns by Chaos Analysis of Pressure Signals. *Chem. Eng. Sci.*, **52**, 4447-4459.

23 Sie, S.T. and Krishna, R. (1998) Process Development and Scale up: II. Catalyst Design Strategy. *Reviews in Chemical Engineering*, 14, 159-202.

24 Sie, S.T. and Krishna, R. (1998) Process Development and Scale up: III. Scale up and Scale down of Trickle Bed Processes. *Reviews in Chemical Engineering*, 14, 203-252.

25 Letzel, H.M., Schouten, J.C., van den Bleek, C.M. and Krishna, R. (1998) Influence of Gas Density on the Large-

Bubble Holdup in Bubble Column Reactors. *AIChE J.*, **44**, 2333-2336.

26 Krishna, R., Van Baten, J.M. and Ellenberger, J. (1998) Scale Effects in Fluidized Multiphase Reactors. *Powder Technology*, 100, 137-146.

27 Sie, S.T. and Krishna, R. (1999) Fundamentals and Selection of Advanced Fischer-Tropsch Reactors. *Applied Catalysis A*, 186, 55-70.

28 Krishna, R., Urseanu, M.I., Van Baten, J.M. and Ellenberger, J. (1999) Rise Velocity of a Swarm of Large Gas Bubbles in Liquids. *Chem. Eng. Sci.*, **54**, 171-183.

29 Krishna, R. and van Baten, J.M. (1999) Simulating the Motion of Gas Bubbles in a Liquid. *Nature*, 398, 208.

30 Krishna, R., Urseanu, M.I. and Dreher, A. (2000) Gas Holdup in Bubble Columns: Influence of Alcohol Addition Versus Operation at Elevated Pressures. *Chem. Eng. & Processing*, 39, 371-378.

31 Letzel, H.M., Schouten, J.C., van den Bleek, C.M. and Krishna, R. (1999) Gas Holdup and Mass Transfer in Bubble Column Reactors Operated at Elevated Pressure. *Chem. Eng. Sci.*, **54**, 2237-2246.

32 Krishna, R., Ellenberger, J. and Maretto, C. (1999) Flow Regime Transition in Bubble Columns. *Int. Commn. Heat Mass Transfer*, 26, 467-475.

33 Krishna, R., Urseanu, M.I., Van Baten, J.M. and Ellenberger, J. (1999) Influence of Scale on the Hydrodynamics of Bubble Columns Operating in the Churn-Turbulent Regime: Experiments vs. Eulerian Simulations. *Chem. Eng. Sci.*, **54**, 4903-4911.

34 Van der Laan, G.P., Beenackers, A.A.C.M. and Krishna, R. (1999) Multicomponent Reaction Engineering Model for Fe-Catalysed Fischer-Tropsch Synthesis in Commercial Scale Bubble Column Slurry Reactors. *Chem. Eng. Sci.*, **54**, 5013-5019.

35 Krishna, R., Urseanu, M.I., Van Baten, J.M. and Ellenberger, J. (1999) Wall Effects on the Rise of Single Gas Bubbles in Liquids. *Int. Commn. Heat Mass Transfer*, 26, 781-790.

36 Maretto, C. and Krishna, R. (1999) Modelling of a Bubble Column Slurry Reactor for Fischer-Tropsch Synthesis. *Catalysis Today*, 52, 279-289.

37 Krishna, R. and van Baten, J.M. (1999) Rise Characteristics of Gas Bubbles in a 2D Rectangular Column: VOF Simulations vs. Experiments. *Int. Commn. Heat Mass Transfer*, 26, 965-974.

38 Krishna, R., Van Baten, J.M. and Urseanu, M.I. (2000) Three-Phase Eulerian Simulations of Bubble Column Reactors Operating in the Churn-Turbulent Flow Regime: A Scale up Strategy. *Chem. Eng. Sci.*, **55**, 3275-3286.

39 Akita, K. and Yoshida Y. (1973) Gas Holdup and Volumetric Mass-Transfer Coefficient in Bubble Columns. *Ind. Eng. Chem. Process Des. Dev.*, **12**, 76-80.

40 Bach, H.F. and Pilhofer, T. (1978) Variation of Gas Holdup in Bubble Columns with Physical Properties of Liquids and Operating Parameters of Columns. *Ger. Chem. Eng.*, **1**, 270-275.

41 Hikita, H., Asai, S., Tanigawa, K. and Kitao, M. (1980) Gas Holdup in Bubble Columns. *Chem. Eng. J.*, 20, 59-67.

42 Hughmark, G.A. (1967) Holdup and Mass Transfer in Bubble Columns. *Ind. Eng. Chem. Process Des. Dev.*, **6**, 218-220.

43 Reilly, I.G., Scott, D.S., De Bruijn, T.J.W., Jain, A.K. and Piskorz, J. (1986) A Correlation for Gas Holdup in Turbulent Bubble Column. *Can. J. Chem. Eng.*, **64**, 705-717.

44 Wilkinson, P.M., Spek, A.P. and Van Dierendonck, L.L. (1992) Design Parameters Estimation for Scale-up of High-Pressure Bubble Columns. *AIChE J.*, **38**, 544-554.

45 Zehner, P. (1989) Mehrphasenströmungen in Gas-Flüssigkeits-Reaktoren. *Dechema Monogr.*, 114, 215-233.

46 Clift, R., Grace, J.R. and Weber, M.E. (1978) *Bubbles, Drops and Particles*, Academic Press, San Diego.

47 Fan, L.S. and Tsuchiya, K. (1990) *Bubble Wake Dynamics in Liquids and Liquid-Solid Suspensions*, Butterworth-Heinemann, Boston.

48 Mendelson, H.D. (1967) The Prediction of Bubble Terminal Velocities from Wave Theory. *AIChE J.*, **13**, 250-253.

49 Davies, R.M. and Taylor, G.I. (1950) The Mechanics of Large Bubbles Rising through Extended Liquids and through Liquids in Tubes. *Proc. Roy. Soc. London*, **A200**, 375-390.

50 Collins, R. (1967) The Effect of a Containing Cylindrical Boundary on the Velocity of a Large Gas Bubble in a Liquid. *J. Fluid Mech.*, 28, 97-112.

51 Richardson, J.F. and Zaki, W.N. (1954) Sedimentation and Fluidisation: Part I. *Trans. Inst. Chem. Eng.*, **32**, 35-53.

52 Harmathy, T.J. (1960) Velocity of Large Drops and Bubbles in Media of Infinite or Restricted Extent. *AIChE J.*, **6**, 281-288.

53 Reilly, I.G., Scott, D.S., De Bruijn, T.J.W. and MacIntyre, D. (1994) The Role of Gas Phase Momentum in Determining Gas Holdup and Hydrodynamic Flow Regimes in Bubble Column Operations. *Can. J. Chem. Eng.*, **72**, 3-12.

54 Bernemann, K. (1989) Zur Fluiddynamik und zum Vermischungsverhalten der flüssigen Phase in Blasensäulen mit längsangeströmten Rohrbundeln. *PhD Thesis*, University Dortmund.

55 Joshi, J.B. (1980) Axial Mixing in Multiphase Contactors–A Unified Correlation. *Trans. Inst. Chem. Eng.*, **58**, 155-165.

56 Kawase, Y. and Moo-Young, M. (1989) Turbulent Intensity in Bubble Column. *Chem. Eng. J.*, 40, 55-58.

57 Nottenkämper, R., Steiff, A. and Weinspach, P.M. (1983) Experimental Investigation of Hydrodynamics of Bubble Columns. *Ger. Chem. Eng.*, **6**, 147-155.

58 Ohki, Y. and Inoue, H. (1970) Longitudinal Mixing of the Liquid Phase in Bubble Columns. *Chem. Eng. Sci.*, **25**, 1-16.

59 Riquarts, H.P. (1981) Strömungsprofile, Impulsaustausch und Durchmischung der flüssigen Phase in Bläsensaulen. *Chem. Ing. Techn.*, 53, 60-61.

60 Ueyama, K. and Miyauchi, T. (1979) Properties of Recirculating Turbulent Two Phase Flow in Gas Bubble Columns. *AIChE J.*, **25**, 258-266.

61 Ulbrecht, J.J., Kawase, Y. and Auyeung, K.F. (1985) More on Mixing of Viscous Liquids in Bubble Columns. *Chem. Eng. Commun.*, 35, 175-191.

62 Zehner, P. (1982) Impuls-, Stoff- und Wärmetransport in Blasensäulen. Teil 1: Strömungsmodell der Blasensäule und Flüssigkeitsgeschwindigkeiten. *Verfahrenstechnik*, 16, 347-351.

63 Baird, M.H.I. and Rice, R.G. (1975) Axial Dispersion in Large Unbaffled Columns. *Chem. Eng. J.*, 9, 171-174.

64 Deckwer, W.D., Burckhart, R. and Zoll, G. (1974) Mixing and Mass Transfer in Tall Bubble Columns. *Chem. Eng. Sci.*, **29**, 2177-2188.

65 Towell, G.D. and Ackerman, G.H. (1972) Axial Mixing of Liquids and Gas in Large Bubble Reactor. *Proc. of 2nd International Symposium Chem. React. Eng.*, Amsterdam, The Netherlands, B3.1-B3.13.

66 Wendt, R., Steiff, A. and Weinspach, P.M. (1984) Liquid Phase Dispersion in Bubble Columns. *Ger. Chem. Eng*., **7**, 267-273.

67 Deckwer, W.D., Serpemen, Y., Ralek, M. and Schmidt, B. (1982) Modeling the Fischer-Tropsch Synthesis in the Slurry Phase. *Ind. Eng. Chem. Process Des. Dev*., **21**, 231-241.

68 Fan, L.S., Yang, G.Q., Lee, D.J., Tsuchiya, K. and Luo, X. (1999) Some Aspects of High-Pressure Phenomena of Bubbles in Liquids and Liquid-Solid Suspensions. *Chem. Eng. Sci*., **54**, 4681-4709.

Final manuscript received in January 2000